# Evaluation of Limited-Area Models for the Representation of the Diurnal Cycle and Contrasting Nights in CASES-99

G. J. STEENEVELD,* T. MAURITSEN,+ E. I. F. DE BRUIJN,# J. VILÀ-GUERAU DE ARELLANO,*
G. SVENSSON,+ AND A. A. M. HOLTSLAG*

*Meteorology and Air Quality Group, Wageningen University, Wageningen, Netherlands
+Department of Meteorology, Stockholm University, Stockholm, Sweden
#Royal Netherlands Meteorological Institute, De Bilt, Netherlands

## ABSTRACT

This study evaluates the ability of three limited-area models [the fifth-generation Pennsylvania State University–National Center for Atmospheric Research Mesoscale Model (MM5), the Coupled Ocean–Atmosphere Mesoscale Prediction System (COAMPS), and the High-Resolution Limited-Area Model (HIRLAM)] to predict the diurnal cycle of the atmospheric boundary layer (ABL) during the Cooperative Atmosphere–Surface Exchange Study (CASES-99) experimental campaign. Special attention is paid to the stable ABL. Limited-area model results for different ABL parameterizations and different radiation transfer parameterizations are compared with the in situ observations. Model forecasts were found to be sensitive to the choice of the ABL parameterization both during the day and at night. At night, forecasts are particularly sensitive to the radiation scheme. All three models underestimate the amplitude of the diurnal temperature cycle (DTR) and the near-surface wind speed. Furthermore, they overestimate the stable boundary layer height for windy conditions and underestimate the stratification of nighttime surface inversions. Favorable parameterizations for the stable boundary layer enable rapid surface cooling, and they have limited turbulent mixing. It was also found that a relatively large model domain is required to model the Great Plains low-level jet. A new scheme is implemented for the stable boundary layer in the Medium-Range Forecast Model (MRF). This scheme introduces a vegetation layer, a new formulation for the soil heat flux, and turbulent mixing based on the local scaling hypothesis. The new scheme improves the representation of surface temperature (especially for weak winds) and the stable boundary layer structure.

## 1. Introduction

Limited-area models (LAM) such as the fifth-generation Pennsylvania State University–National Center for Atmospheric Research (PSU–NCAR) Mesoscale Model (MM5; Dudhia and Bresch 2002), the Coupled Ocean–Atmosphere Mesoscale Prediction System (COAMPS; Hodur 1997), and the High-Resolution Limited-Area Model (HIRLAM; Undén et al. 2002) are used for operational short-range regional weather forecasting, to predict air pollution episodes (Hanna and Yang 2001, hereinafter HY01), to reconstruct regional budgets of several trace gases (e.g., $CO_2$, Aalto

et al. 2006), and for atmospheric research. It is important for many applications that LAMs predict correctly the profiles of potential temperature ($\theta$), specific humidity ($q$), trace gases and wind speed and direction, as well as surface turbulent and radiation fluxes. To achieve this we need to include the relevant physical processes in the atmospheric boundary layer (ABL) within LAMs.

At midlatitudes, the ABL undergoes a clear diurnal cycle (Betts 2001). Daytime insolation heats the surface and a turbulent heat flux is directed toward the atmosphere. The ABL is well mixed by convection, which transports heat, moisture, and scalars upward from the surface. ABL top entrainment also affects $\theta$ and $q$ inside the ABL (e.g., Stull 1988; Holtslag et al. 1995; Steeneveld et al. 2005). In contrast, at night, the ABL is not well mixed and strong vertical gradients in wind speed and temperature are observed. Besides turbulent

Corresponding author address: Gert-Jan Steeneveld, Meteorology and Air Quality Group, Wageningen University, P.O. Box 47, 6700 AA Wageningen, Netherlands.
E-mail: gert-jan.steeneveld@wur.nl

mixing, the impact of radiation divergence (e.g., Ha and Mahrt 2003) and the feedback from the underlying soil and vegetation is also evident for stable conditions (Holtslag and de Bruin 1988; Beljaars 2001; Steeneveld et al. 2006, hereinafter S06). Moreover, a low-level jet (LLJ) can develop at night (e.g., Song et al. 2005), which can contribute to the ABL turbulent structure. In general, the structure of the stable boundary layer (SBL) is more complicated and more variable than the structure of the daytime ABL (Mahrt 1998, 1999; Mahrt et al. 1998), making it more difficult to model.

Recent LAM evaluation studies have focused on specific topics such as complex terrain (Zhong and Fast 2003; Berg and Zhong 2005), Arctic (Tjernström et al. 2004) or Antarctic regions (e.g., King et al. 2001), air pollution episodes (HY01), tropical cyclone formation (Braun and Tao 2000), the American monsoon (Bright and Mullen 2002), or the convective boundary layer (CBL; Vilà-Guerau de Arellano et al. 2001). Less attention has been paid to model representation of the diurnal cycle (Zhang and Zheng 2004), although its representation in models is rather problematic (Beljaars 2001; Holtslag 2006). Moreover, the representation of the SBL in LAMs has not been comprehensively evaluated. Good representation of the diurnal cycle and the SBL is a key issue for numerical weather prediction (NWP) and regional climate modeling, for air quality studies, wind energy engineering, and atmospheric research.

Considerable progress has been made in ABL parameterizations for NWP and climate modeling. However, the SBL is relatively poorly understood and modeled (Beljaars 1995; King and Connolley 1997; Savijärvi and Kauhanen 2001; Cassano et al. 2001; Cuxart et al. 2006), since it is driven by two distinct physical processes: turbulence and radiative cooling. Additional processes such as gravity waves, intermittent turbulence, density currents, and katabatic winds could play an important role, as well as the effects of land surface heterogeneity. Consequently stationarity and homogeneity are usually absent at night, and parameterizations often fail (e.g., Holtslag 2006).

This study extends previous work by evaluating three LAMs focusing on the representation of the diurnal cycle, and the SBL in particular. Because of the complexity of the SBL itself, we limit ourselves to three selected consecutive clear days, over relatively simple topography during the Cooperative Atmosphere–Surface Exchange Study (CASES-99) experimental campaign.

Previous studies mainly addressed the sensitivity to turbulence schemes. Here we also discuss the sensitivity to the radiation scheme, because both processes play a
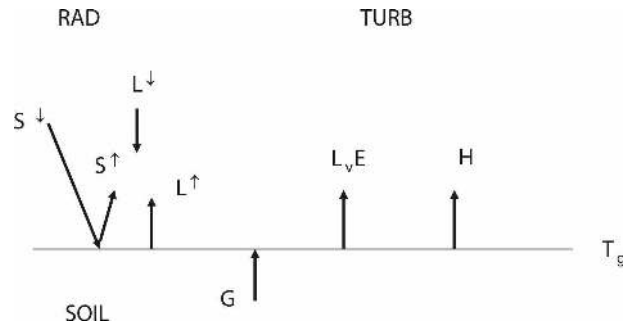


FIG. 1. Illustration of the interaction between the energy fluxes by different physical processes in the SBL. The surface temperature $T_g$ plays a central role in the SBL physics with its direct impact and feedbacks on the turbulence, radiative transport, and the land surface. Here $S$ is solar radiation, $L$ is longwave radiation, $H$ is sensible heat flux, $L_v E$ is latent heat flux, and $G$ is soil heat flux.

key role in predicting the diurnal cycle. As such the interplay between the turbulence, radiation, and land surface is also considered through the surface vegetation temperature $T_{veg}$ (Fig. 1). Since $T_{veg}$ (together with the air temperature $T_a$) governs the atmospheric stability, it also governs the turbulence intensity. Moreover, the nighttime near-surface clear air radiative cooling appears to be proportional to $T_a - T_{veg}$. Finally, the difference between $T_{veg}$ and the soil temperature governs the soil heat flux ($G$). Thus, $T_{veg}$ plays a key role for the surface energy budget and is therefore more critical than the 2-m temperature.

Since many permutations of both the surface layer, ABL, and land surface schemes are considered in the current study, our strategy is to 1) search for common deficiencies in all models, and 2) to examine whether a certain model description is advantageous under certain atmospheric conditions. From this we can learn how to improve those that perform less well in those conditions. Also LAMs other than those considered in our study may benefit from our findings. Finally, we implement an improved scheme for the SBL in MM5. This scheme introduces a vegetation layer to the land surface scheme, a more realistic formulation for $G$, and local mixing at night. The new scheme provides a much better representation of $T_{veg}$ and the SBL vertical structure (especially for weak winds).

This study aims to examine whether ABL parameterizations in different LAMs, are able to forecast the mean thermodynamic profiles correctly, and consistently with the surface turbulent and radiation flux calculations (especially for the SBL). We compare widely used ABL schemes in MM5, COAMPS, and the HIRLAM version operational at the Royal Netherlands Meteorological Office (KNMI) on three contrasting diurnal cycles during the CASES-99 campaign:

calm, moderately windy, and strong wind conditions (as in S06). Finally, we improve the performance of MM5 for the SBL by implementing a vegetation layer, local mixing at night, and a more realistic formulation for the soil heat flux.

## 2. Observations and synoptic conditions

### a. Observations

For this study we select the period 23–26 October 1999 during the CASES-99 campaign (Poulos et al. 2002), which has been analyzed before in the context of a column model study in S06. This period has been chosen because the nights differ strongly in turbulence intensity. The first night is intermittently turbulent, the second is fully turbulent, and the third is hardly turbulent and mainly driven by radiative cooling (S06). The experiment has been conducted near Leon, Kansas (37.65°N, 96.73°W, 436 m MSL). The area consists of gently rolling homogeneous terrain with a relatively dry soil, and lacks obstacles in the near surroundings. The area consists of prairie grass, and has a roughness length for momentum ($z_0$) of 0.03 m.

Ground-based observations consist of $\theta$, $q$, and wind profiles along a 60-m tower (mounted at 1.5, 5, 10, . . . , 55 m), and turbulent and radiative fluxes near the surface. The eddy-covariance measurements of the surface sensible heat flux, latent heat flux, and friction velocity were obtained at 2.6 m. Here $G$ has been obtained as in van de Wiel (2002). The surface energy budget closure is approximately 100% for these nights (S06). Additionally, sodar observations and irregularly launched radiosondes provided information on upper-air characteristics and the ABL height ($h$), here taken arbitrarily as the height of 8-dB sodar signal reflection. Alternative $h$ derived from turbulence observations along the 60-m tower are also used (Vickers and Mahrt 2004). As such, this unique and extensive dataset is excellent evaluation material for the current study.

### b. Synoptic conditions

The three selected nights have a moderate, strong, and very weak synoptic forcing, respectively (Fig. 2). During the first night the CASES-99 site is located under a high pressure system with a geostrophic wind
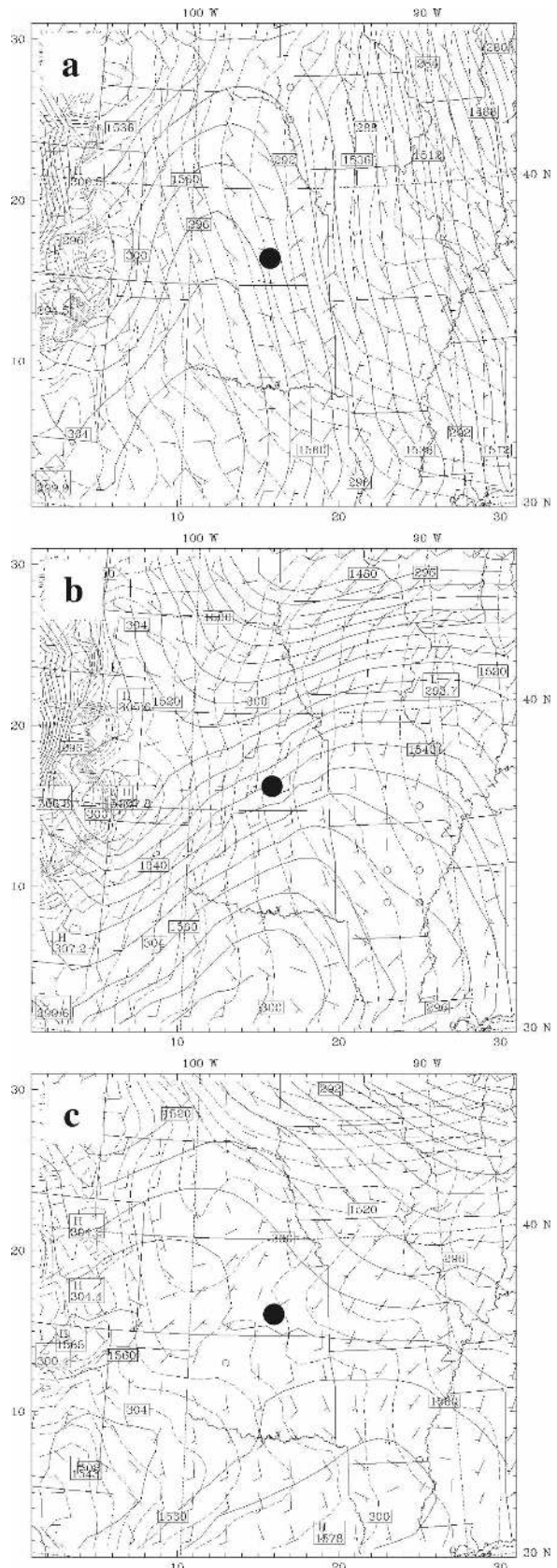
$\rightarrow$



FIG. 2. Synoptic overview at 0600 UTC (0000 LT) for the three considered diurnal cycles: (a) 24, (b) 25, and (c) 26 Oct. The 850-hPa geopotential height (black line), 850-hPa potential temperature (dashed line), and 10-m wind speed (vector) as forecast by the MM5-MRF scheme are plotted. CASES-99 site is in the middle of the domain and is marked with the black dot.
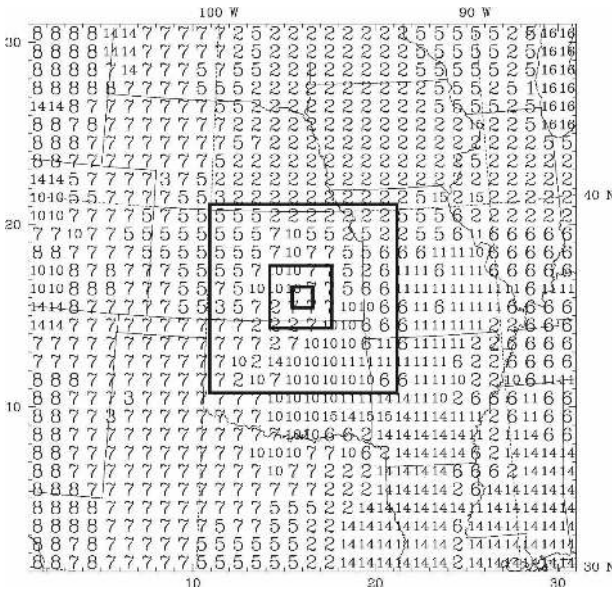
FIG. 3. Model domain configuration (total size 1620 km × 1620 km) and land use (2 = dryland, cropland, and pasture; 5 = cropland/grassland mosaic; 6 = cropland/woodland mosaic; 7 = grassland; 8 = shrubland; 10 = savanna; 14 = evergreen needleleaf forest; 16 = water).

speed ~6 m s$^{-1}$. The near-surface turbulence is of intermittent character during this night. During the second night a trough is west of the measurement site (Fig. 2b), which coincides with increasing geostrophic forcing in time and heat advection. At about 200 m AGL a typical Great Plains LLJ of 21 m s$^{-1}$ was observed (Banta et al. 2002). A weak front passes at the end of the night, which was most clearly seen in the $q$ increase from ~2.5 to ~6 g kg$^{-1}$, although no clouds were observed. In the last night, the site is under a high pressure area, and the geostrophic wind speed is about 4 m s$^{-1}$, and decreases at night. Advection is absent and radiative cooling plays an important role in the SBL during this night.

# 3. Model descriptions and configurations

## a. Configuration

The LAMs are run for a 1620 km × 1620 km area over the central part of the United States. (Fig. 3). MM5 and COAMPS use 31 × 31 grid points with a grid spacing in the outer domain of 54 and 49 km, respectively. Three smaller domains (also 31 × 31 nodes) with a resolution of 18, 6, and 2 km are nested inside this domain to avoid model errors from coarse resolution. HIRLAM uses 10-km horizontal resolution without nesting in the whole domain, covering nearly the entire United States. Although the three models do not have exactly the same horizontal resolution, they all use a

very high resolution. Since land surface properties are rather homogeneous in this region, significant improvement from increased resolution should not be expected. This was confirmed from coarse grid MM5 and COAMPS simulations, where the results from the 2- and 6-km nests are nearly identical.

The U.S. Geological Survey (USGS) provides the land surface characteristics (Zehnder 2002). Because local observations of $z_0$ and soil moisture ($M$) were available, we prescribed $z_0 = 0.03$ m and $M = 0.08$ for the relevant land-use types. MM5 employed 36 terrain-following $\sigma_p$ levels (22 layers are in the lowest 2 km), COAMPS used 50 $\sigma_z$ levels, and HIRLAM used 40 hybrid layers. Initial and boundary conditions for atmospheric variables are taken from the European Centre for Medium-Range Weather Forecasts (ECMWF; 1° × 1°) operational analysis every 6 h. No data assimilation of surface and upper-air observations has been performed during the simulations, and the models use a 24-h spinup. We will analyze the period of 1800 UTC 23 October–1800 UTC 26 October.

## b. Model physics

The relevant model components to model the ABL are the surface layer scheme, the ABL scheme, the radiation scheme, and the land surface scheme. We briefly describe these model components (see the appendix for more details). With the current models we obtain the permutations summarized in Table 1. This study uses the PSU–NCAR MM5 (v3.6.1) model (Dudhia et al. 2000), COAMPS (v3.1.1), and HIRLAM (v7.0.1). In MM5, four ABL schemes were selected: the Medium-Range Forecast (MM5-MRF; Troen and Mahrt 1986; Holtslag and Boville 1993; Hong and Pan 1996), the ETA-Mellor–Yamada scheme (MM5-ETA; Janjić 1990), Blackadar (MM5-BLA), and Burk–Thompson (1989; MM5-BT). These schemes were selected because of their different physical assumptions and their common use in atmospheric models. For completeness, we note that MM5 uses the Dudhia (1989) CLOUD radiation scheme, while COAMPS and HIRLAM use the schemes by Harshvardhan et al. (1987) and Savijärvi (1990), respectively. MM5 and COAMPS use the Kain and Fritsch (1993) convection scheme, whereas HIRLAM uses the Soft Transition Condensation (STRACO) scheme (Undén et al. 2002).

### 1) SURFACE LAYER

All schemes calculate the surface fluxes of heat ($H$) and momentum ($\tau$) according to

$$H = C_p C_\theta \rho_a U(\theta_{vg} - \theta_{va}) \qquad (1)$$

and

TABLE 1. Overview of model parameterizations in the surface layer, boundary layer, and for the land surface in the current intercomparison.

| Model | Surface layer | Boundary layer | Surface/vegetation |
|---|---|---|---|
| MM5-MRF | MO-short tail | $K$ profile (nonlocal daytime) | Five soil layers–no vegetation layer |
| MM5-BLA | MO-short tail | Local $K$ theory (for stable) Nonlocal (for unstable) | Five soil layers–no vegetation layer |
| MM5-ETA | MO-short tail | TKE-$l$: $l = kz/(1 + kz/l_\infty)$ | Five soil layers–no vegetation layer |
| MM5-BT | Louis | TKE-$l$: $l = kz/(1 + kz/l_\infty)$ | Force–restore + vegetation layer |
| HIRLAM | Louis | TKE-$l$: $1/l = 1/(c_n kz) + 1/(\sqrt{TKE}/N)$ [details Eqs. (5)–(7)] | ISBA: force–restore with vegetation layer |
| COAMPS | Louis | TKE-$l$: $l = kz/(1 + kz/l_\infty)$ | Slab model |

$$\tau = C_D \rho_a U^2. \tag{2}$$

Here $C_p$, $\rho_a$, and $U$ are the specific heat of air, the air density, and near-surface wind speed, respectively. The $C_\theta$ and $C_D$ are the stability-dependent exchange coefficients for heat and momentum, and $\theta_{vg}$ and $\theta_{va}$ are the virtual potential temperatures at the surface and the air. We distinguish between two different formulations for $C_\theta$ and $C_D$. One type is based on Monin–Obukhov similarity theory (not allowing transfer if the Richardson number Ri is above its critical value $\text{Ri}_{crit}$), used by MM5-MRF, MM5-ETA, and MRF-BLA. The other type is based on the Louis (1979) approach (allowing for mixing for Ri > $\text{Ri}_{crit}$), which is used in COAMPS, HIRLAM, and MM5-BT.

### 2) BOUNDARY LAYER

Within the ABL schemes we can also distinguish between two types. In the first type the turbulent diffusion is based on nonlocal closure during the day and the Louis scheme at night. The nonlocal closure enhances the daytime mixing, which usually results in a better performance relative to local schemes (Holtslag et al. 1995). As such, these schemes provide more realistic initial conditions for the night. At night nonlocal transport should be zero since large eddies are absent.

The second type is a 1.5-order [level 2.5 in the Mellor and Yamada (1974) hierarchy] closure model and solves the budget equation for turbulent kinetic energy ($E$), with the exchange coefficient $K$ that depends on Ri via complicated algebraic functions $S_{M,H}$:

$$K = l\sqrt{E}f(\text{Ri}). \tag{3}$$

The length scale $l$ specification plays a key role, and is usually given by

$$l^{-1} = (kz)^{-1} + l_\infty^{-1}, \tag{4}$$

with $k$ the von Kármán constant and $l_\infty$ an asymptotic mixing length. HIRLAM uses an extra length scale to account for stability, instead of correction via $f$:

$$l^{-1} = [\max(l_{int}, l_{min})]^{-1} + l_s^{-1}, \tag{5}$$

with $l_{int}$ being an integral length scale only used for the daytime, and

$$l_s = c_{m,h}\sqrt{E}/N. \tag{6}$$

TABLE 2. Statistical model evaluation for the reference runs based on the full time series. Boldface numbers indicate the best score for a particular quantity and statistical measure.

| | Model | Bias | MAE | RMSE | FB | Corr | IoA |
|---|---|---|---|---|---|---|---|
| $T_{veg}$ | COAMPS | −1.37 | **2.31** | **2.94** | −0.11 | **0.980** | **0.981** |
| $u_*$ | COAMPS | 0.08 | **0.09** | 0.11 | 0.38 | **0.854** | 0.802 |
| $H$ | COAMPS | 5.69 | 22.00 | 30.96 | 0.15 | **0.982** | 0.957 |
| $L_vE$ | COAMPS | **2.13** | **4.42** | **6.55** | **0.14** | **0.940** | **0.964** |
| $L^\downarrow$ | COAMPS | −25.27 | 25.89 | 28.31 | −0.09 | 0.834 | 0.625 |
| $L^\uparrow$ | COAMPS | 3.40 | **8.45** | **10.60** | 0.01 | **0.984** | **0.990** |
| $T_{veg}$ | MM5-MRF | **0.63** | 4.16 | 4.67 | **0.05** | 0.951 | 0.939 |
| $u_*$ | MM5-MRF | 0.09 | 0.095 | 0.13 | 0.43 | 0.783 | 0.760 |
| $H$ | MM5-MRF | −5.51 | 15.95 | 23.91 | −0.20 | 0.951 | 0.974 |
| $L_vE$ | MM5-MRF | 3.94 | 6.96 | 9.70 | 0.29 | 0.876 | 0.907 |
| $L^\downarrow$ | MM5-MRF | 6.31 | 10.14 | 11.95 | 0.02 | 0.863 | 0.906 |
| $L^\uparrow$ | MM5-MRF | **0.73** | 17.58 | 20.44 | **0.002** | 0.959 | 0.951 |
| $T_{veg}$ | MM5-ETA | −0.69 | 4.01 | 4.87 | −0.06 | 0.950 | 0.934 |
| $u_*$ | MM5-ETA | 0.08 | **0.09** | 0.12 | 0.41 | 0.800 | 0.781 |
| $H$ | MM5-ETA | −3.47 | 15.61 | 22.83 | −0.12 | 0.954 | 0.977 |
| $L_vE$ | MM5-ETA | 8.55 | 10.92 | 15.89 | 0.53 | 0.873 | 0.750 |
| $L^\downarrow$ | MM5-ETA | **0.92** | **8.90** | 11.54 | **0.003** | 0.817 | 0.912 |
| $L^\uparrow$ | MM5-ETA | −6.15 | 17.50 | 22.69 | −0.017 | 0.957 | 0.939 |
| $T_{veg}$ | MM5-BLA | 0.75 | 4.18 | 4.63 | 0.06 | 0.951 | 0.940 |
| $u_*$ | MM5-BLA | 0.12 | 0.13 | 0.16 | 0.57 | 0.804 | 0.632 |
| $H$ | MM5-BLA | −7.60 | 17.69 | 26.24 | −0.29 | 0.943 | 0.969 |
| $L_vE$ | MM5-BLA | 5.20 | 8.32 | 11.03 | 0.36 | 0.846 | 0.880 |
| $L^\downarrow$ | MM5-BLA | 6.15 | 9.41 | 11.44 | 0.02 | **0.871** | 0.914 |
| $L^\uparrow$ | MM5-BLA | 1.34 | 17.61 | 20.09 | 0.004 | 0.959 | 0.952 |
| $T_{veg}$ | MM5-BT | −1.42 | 3.11 | 4.20 | −0.13 | 0.970 | 0.950 |
| $u_*$ | MM5-BT | 0.08 | **0.09** | 0.12 | 0.40 | 0.804 | 0.788 |
| $H$ | MM5-BT | **1.15** | **15.21** | 23.09 | **0.038** | 0.957 | 0.976 |
| $L_vE$ | MM5-BT | 7.43 | 10.15 | 16.38 | 0.48 | 0.885 | 0.734 |
| $L^\downarrow$ | MM5-BT | 3.15 | 8.92 | **11.00** | 0.011 | 0.843 | **0.920** |
| $L^\uparrow$ | MM5-BT | −9.60 | 13.79 | 20.04 | −0.026 | 0.974 | 0.953 |
| $T_{veg}$ | HIRLAM | −2.12 | 4.51 | 3.70 | −0.19 | 0.956 | 0.937 |
| $u_*$ | HIRLAM | **−0.04** | **0.09** | **0.08** | **−0.29** | 0.693 | **0.842** |
| $H$ | HIRLAM | −0.14 | 17.71 | **12.27** | 0.00 | 0.975 | **0.986** |
| $L_vE$ | HIRLAM | 3.01 | 9.08 | 6.91 | 0.21 | 0.937 | 0.918 |
| $L^\downarrow$ | HIRLAM | −24.60 | 12.60 | 25.03 | −0.09 | 0.800 | 0.565 |
| $L^\uparrow$ | HIRLAM | −14.28 | 21.30 | 18.52 | −0.04 | 0.961 | 0.930 |
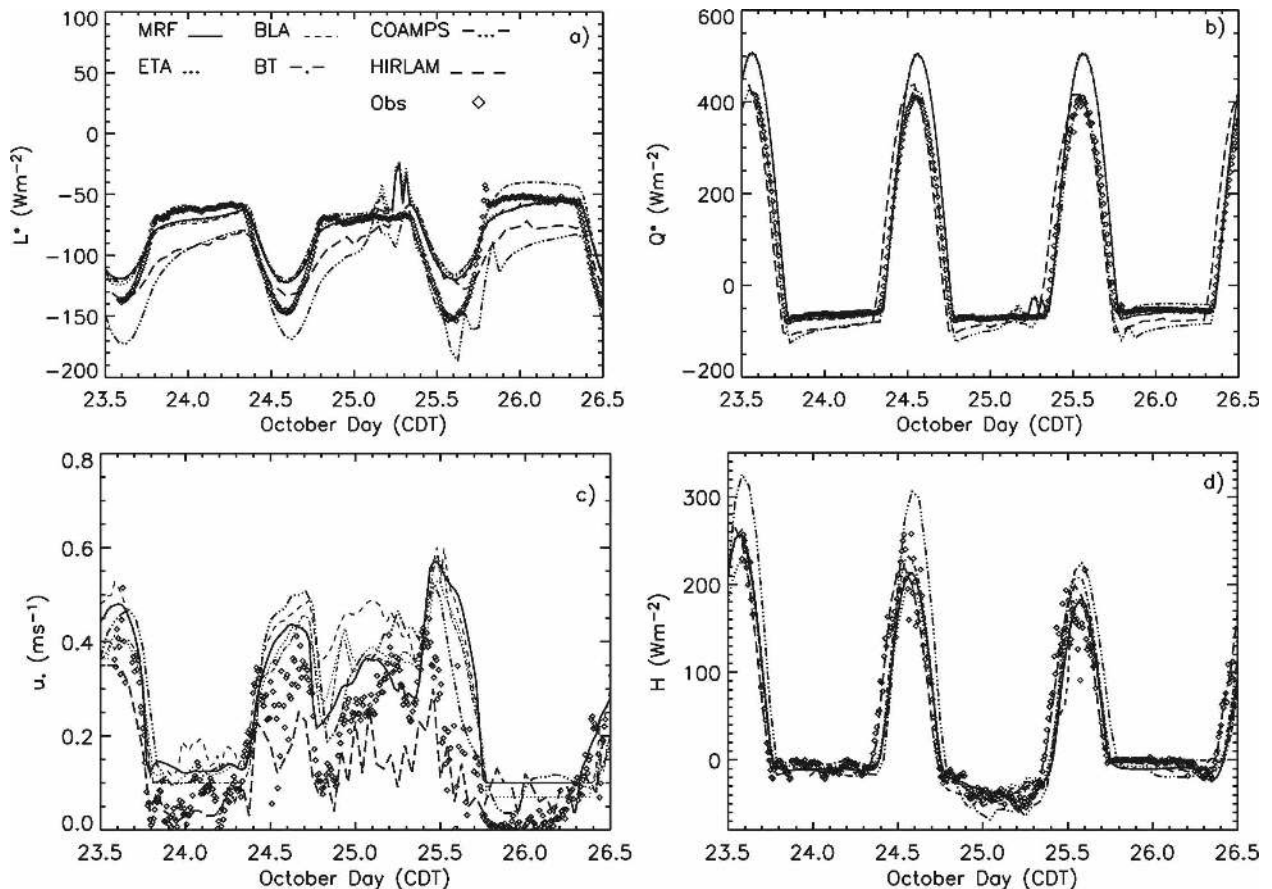
FIG. 4. Time series of modeled and observed (a) longwave net radiation, (b) net radiation, (c) friction velocity, (d) surface sensible heat flux, (e) zoomed-in surface sensible heat flux, (f) vegetation surface temperature, and (g) boundary layer height.

Here $c_h = 0.2$ and $c_m = 4\,c_h$, and $N$ is the local Brunt–Väisälä frequency, and

$$l_{\min}^{-1} = (c_n k z)^{-1} + l_{\lim it}^{-1}, \qquad (7)$$

with $c_n = 0.5$ (Lenderink and Holtslag 2004; Tijm 2004). Within each approach $f(\mathrm{Ri})$ is based on either the Monin–Obukhov type or the Louis type.

### 3) LAND SURFACE

Within the land surface schemes, we can generally distinguish between models that use the force–restore method (Deardorff 1978) and those with a multilayer scheme that solve the diffusion equation for heat. Second, the models use different heat capacities of the first soil–vegetation layer, some accounting for the small heat capacity of the vegetation. HIRLAM utilizes the Interactions between Soil, Biosphere, and Atmosphere (ISBA) land surface scheme, with a vegetation layer (Noilhan and Mahfouf 1996). MM5-BT is the only scheme that does not use the multilayer scheme in MM5, but applies a force–restore method with a veg-

etation layer of small heat capacity on top. COAMPS also uses a force–restore method, but with a slower coupling with the atmosphere.

## 4. Surface temperature and fluxes

In this section we focus on the model results for turbulent and radiative surface fluxes. Table 2 provides an overview of statistical measures for model performance [i.e., bias, mean absolute error (MAE), root-mean-square error (RMSE), fractional bias (FB), correlation coefficient, and the index of agreement (IoA, a modified correlation coefficient, that accounts for phase errors between modeled ($MOD_i$) and observed ($OBS_i$) time series; Willmott 1982].

### a. Surface radiation

Both COAMPS and MM5 (for all ABL schemes) overestimate the net surface solar radiation by 50 and 25 W m$^{-2}$, respectively (not shown in Table 2). This may be partly explained by a dry bias in the initial $q$ field provided by ECMWF. An underestimation of $q$
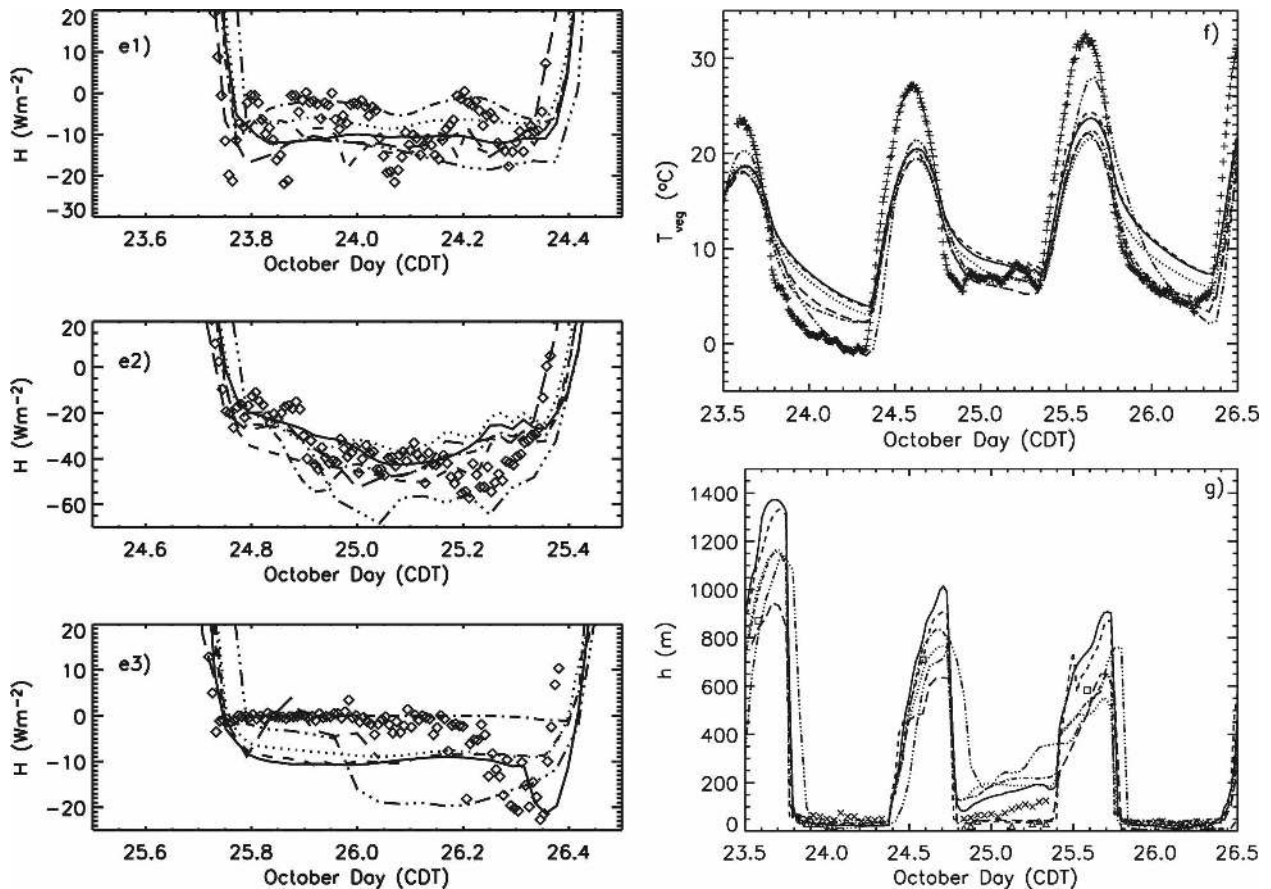
FIG. 4. (*Continued*)

enhances shortwave downwelling radiation, and underestimates of downwelling longwave radiation ($L^\downarrow$). The modeled longwave net radiation ($L^*$, Fig. 4a) with MM5 is close to the observations (maximum bias 20 W m$^{-2}$ in the first night) with the best estimate by the BT scheme. MRF and BLA perform rather similarly. However, during the daytime $L^*$ is underestimated because of underestimated $T_{veg}$ and thus $L^\uparrow$ (Fig. 4f), except for COAMPS, which forecasts a slightly higher $T_{veg}$ than MM5. COAMPS and HIRLAM have negative $L^*$ bias of ~30–40 and ~20 W m$^{-2}$, respectively, especially at night. In the radiative night (25–26 October), MM5-BT slightly underestimates the magnitude of $L^*$ while other MM5 schemes show good correspondence with observations. A closer look to both $L^\downarrow$ and outgoing longwave fluxes ($L^\uparrow$) reveals that the bias of COAMPS in the net radiation is due to continuous underestimation of $L^\downarrow$ (~30 W m$^{-2}$, see Table 2), which is consistent with the dry bias aloft and cold ABL bias in COAMPS. MM5 estimates $L^\downarrow$ reasonably, except for 24 October during the day where MM5 overestimates $L^\downarrow$. This is probably caused by the $q$ profile that differs strongly

between MM5 and the observations (Fig. 6). MM5 is too humid relative to the radiosonde observations and predicts the trough passage earlier than observed. Additionally, since the soil moisture content is low, both the observed and modeled $L_vE$ at the surface are relatively small (50 W m$^{-2}$). Therefore, the relative contribution by entrainment of moist and warm air from the free atmosphere into the ABL can be large (e.g., Couvreux et al. 2005) and the entrainment process has a dominant impact on the $q$ distribution in the ABL. In general MM5-MRF and MM5-BLA have a vigorous entrainment, and TKE models underestimate the entrainment. Note that HIRLAM is also too moist, but this is because of the overestimated $L_vE$. Except for humidity, sources of the $L^\downarrow$ bias can also be due to the parameterization itself (e.g., nearly all radiation codes underestimate $L^\downarrow$ because of the inaccurate treatment of the water vapor continuum) or the codes need more resolution than used here.

The $L^\uparrow$ is mainly governed by $T_{veg}$. MM5 underestimates $L^\uparrow$ during daytime but overestimates $L^\uparrow$ at night. COAMPS shows a time delay with the observations of

about 1 h at noon, due to the large response time of $T_{veg}$ in the land surface scheme. COAMPS has a larger diurnal cycle of $L^{\uparrow}$ than MM5, and performs well for $L^{\uparrow}$ (Table 2). Net radiation (Fig. 4b) is well estimated during daytime by COAMPS and by MM5 at night. COAMPS underestimates net radiation by ~50 W m$^{-2}$ (even more in the last night) which will have serious consequences for the SBL structure.

### b. Turbulent surface fluxes

Friction velocity $u_*$ (see Fig. 4c), is well forecast on 24 October by ETA and BT and overestimated by MRF, BLA, and COAMPS. In the following intermittently turbulent night (24–25 October) all schemes tend to overestimate $u_*$ slightly, and are unable to mimic the intermittent events. Most models fail to reduce $u_*$ during the day–night transitions of 24–25 October and $u_*$ falls too late in the transition of 25–26 October. Finally, $u_*$ is heavily affected by unphysical limiting values in MM5 for strong stability, and strongly overestimated by COAMPS, a common problem with the Louis (1979) scheme. The high $u_*$ in COAMPS coincides with very steep $U$ and $\theta$ profiles between the surface and the lowest model level (Fig. 7), which indicates the effect of an unphysical fix.

HIRLAM is the only model that is able to forecast small $u_*$ in the first night (weak wind), but underestimates $u_*$ during daytime and during the windy night (24–25 October). The small nighttime $u_*$ contradicts with usual findings that the Louis scheme overestimates $u_*$. Scale analysis of the two terms in HIRLAMs length scale formulation [Eqs. (5)–(7)] showed that both terms are of same order of magnitude close to the ground in calm nights, and thus the second term considerably reduces $l$. Additionally, we show that MM5-BT and HIRLAM gives stronger surface cooling at night than the other models, and also limits the turbulence and thus $u_*$. Therefore HIRLAM outperforms for $u_*$ for most statistical parameters (Table 2).

The sensible heat flux ($H$, Figs. 4d,e) is best represented by MM5 and HIRLAM during daytime, where COAMPS overestimates $H$ by 50 W m$^{-2}$ as a result of overestimated incoming solar radiation. During the night of 23–24 October the TKE schemes calculate the smallest $H$, and all schemes are in the observed range (Fig. 4e). The intermittent character of the observed fluxes is absent in all model forecasts. During the night of 24–25 October, all models with the Louis scheme in the surface layer (COAMPS and MM5-BT) overestimate $|H|$, corresponding to earlier findings (van den Hurk and Holtslag 1997; Kot and Song 1998). In the radiative driven night (25–26 October) most models seriously overestimate $|H|$, except HIRLAM and BT. We

will see below that those schemes permit the land surface to cool more rapidly, enhancing the stratification, which is beneficial to the forecast $H$. Only MRF shows that the flux increase before dawn. Based on the full diurnal cycle, HIRLAM gives the largest IoA (0.986).

Latent heat fluxes ($L_v E$) are only 50 W m$^{-2}$ at noon and well represented by MRF, BLA, and COAMPS (IoA = 0.964, Table 2). ETA, BT, and HIRLAM overestimate $L_v E$ by 25 W m$^{-2}$. At night, both the modeled and observed fluxes are small (not shown).

The $T_{veg}$ is a peculiar but important quantity to predict, because of its central role in driving the schemes (Figs. 1 and 4f). All MM5 schemes overestimate the nighttime $T_{veg}$ during weak winds (23–24 and 25–26 October), although this warm bias is smaller for MM5-BT. HIRLAM also corresponds well to observations during these calm nights. Although Zhong and Fast (2003) indicate that the limited resolution might be responsible for the temperature bias, here we point to land surface scheme design. Their remark that with increased resolution or different ABL schemes the surface inversion strength remains too small, implicitly shows that issues other than resolution and the ABL scheme might be responsible for the biased surface inversion strength (e.g., the land surface scheme).

The BT scheme uses a force–restore method with vegetation layer, instead of the five-layer soil model. The use of a vegetation layer is beneficial for the forecast cooling rate. COAMPS forecasts the largest diurnal cycle amplitude, but reaches the minimum temperature too slowly, since the surface cools insufficiently fast. The *warm* bias in most schemes contradicts the *cold* bias found by Zhong and Fast (2003), who attribute the vanishing of the modeled turbulence for this large cooling. However, the turbulence schemes provide several artificial fixes (e.g., minimum $U$, $u_*$, $E$, or maximum $z/L$) to maintain turbulence at strong stability such that a warm bias is expected. Moreover, the surface cooling responds on a long time scale that is different from the time scale of fluctuations of $H$ (i.e., the short time scale). This stresses that the surface properties (i.e., the soil equivalent depth) govern the surface cooling.

Zhang and Zheng (2004) also found an underestimation of the diurnal temperature cycle (DTR), although in their case this was solely present during daytime, while here also the nighttime contribution is substantial. They also found that MM5-BT shows the smallest DTR, and in general a cold bias of typically 2 K at night, while here BT forecast the largest DTR within MM5. Note, however, that Zhang and Zheng (2004) do not report any verification of $L_v E$. If, in their case, the modeled daytime $L_v E$ was too large, a DTR underes-

timation is consistent. A cool daytime bias can then persist at night. In the present study, the $L_vE$ is in close agreement with the observations, and the bias for the CBL bulk temperature is small for the best models.

Zhang and Zheng (2004) report a systematic overestimation of the near-surface wind speed at night and an underestimation during daytime, but this is not found here. The former study also reports substantial phase errors of the near surface wind. In the current study only MRF is some hours ahead from its daytime wind speed maximum.

Since all models use their own internal definition $h$, a clean comparison of $h$ is not possible from direct model output. Therefore, we initially calculated $h$ from the modeled atmospheric profiles a posteriori using the Troen and Mahrt (1986) method, with $Ri_{crit} = 0.25$. However, this method provides ABLs that are too deep for stable conditions, and is thus a less useful method for intercomparison. Therefore, for stable conditions we use the method in Vogelezang and Holtslag (1996) with $Ri_{crit} = 0.3$ to obtain $h$. During the daytime, $h$ is typically 850 m for the last 2 days, but with a large spread, ranging between 650 and 900 m between different schemes (Fig. 4g). MM5-MRF forecasts the deepest CBL. The single observation of $h$ during daytime is insufficient to indicate which model is favorable. COAMPS exhibits a delay of the CBL collapse, caused by the relatively slow surface cooling in this model.

Surprisingly, all models predict $h$ correctly at night during weak winds (23–24 and 25–26 October). This contradicts with earlier findings that $h$ is typically overestimated by about a factor of 2 by this type of model (HY01). For the second night (24–25 October), MRF, ETA, COAMPS, and BT overestimate $h$ with 75–150 m, although $dh/dt$ is reasonably estimated. The disagreement between findings for weak winds and those in HY01 might result from the chosen method to calculate $h$. We obtained similar conclusions as HY01 with the Troen and Mahrt (1986) method. However, the current method showed significantly more skill against Cabauw tower observations, and should therefore be preferred. Note that the estimate of $h$ in this range could also be sensitive to the distribution of the model layers.

## 5. Atmospheric profiles

### a. Diurnal cycle

Figure 5 shows the temporal structure of modeled $\theta$ and wind speed. Although the figure does not provide a direct test against observations, it provides a comparison between the outcome of the model approaches, which gives a more complete picture than comparing

some instantaneous profiles only. First, the incoming heat advection on 25 October is easily seen following the 292-K isentrope, which reaches a lower altitude between the October days 24.7 and 25.0. HIRLAM and COAMPS show a corresponding advection rate over a deep layer, where in MM5 the advection is more slowly in time (the slope of the isentropes is smaller). MRF and BLA provide a rather similar temperature structure in the CBL with a very fast growth in the morning, and a deeper CBL than in other schemes. At night the TKE models mix the cool air at the ground over a shallower layer, especially during the weak wind nights. On the contrary, MRF and BLA mix the cold air over an unrealistically deep layer, and thus do not have a clear residual layer, while HIRLAM limits the cooling to a very shallow layer close to the surface.

A clear wind speed minimum at 500 m AGL is seen before dawn of 25 October, although this is accompanied by a wind maximum close to the surface. All schemes in MM5 produce a LLJ of about 16 m s$^{-1}$ the second night (24–25 October). BLA has the jet typically at a higher altitude than MRF, and the TKE models produce a wind maximum over a deep layer, and a sharp wind speed maximum is only present in HIRLAM and COAMPS. During the last night (25–26 October) all MM5 schemes give a weak LLJ, although they differ in timing. Again, COAMPS provides a deep jet layer while HIRLAM lacks a LLJ.

Similar figures (not shown) for $E$ revealed that the TKE models predict significant different $E$ values in the ABL during daytime, ranging from ~0.9 J kg$^{-1}$ for ETA and COAMPS to ~1.6–2 J kg$^{-1}$ for HIRLAM and MM5-BT for 25 October. Next, we evaluate $U$ and $\theta$ profiles against in situ observations for the CBL and SBL, respectively.

### b. Convective boundary layer

As an illustrative example (Fig. 6), we show the 700-m-deep CBL of 1900 UTC 24 October (which is after the initial effects of the spinup and before strong advection). In correspondence with earlier verifications (e.g., Hong and Pan 1996), the TKE closure models show a shallower and more humid ABL than the nonlocal schemes that forecast the CBL temperature well. MRF and BLA are 0.5 g kg$^{-1}$ too humid because of the excessive entrainment of moist air from the free atmosphere. HIRLAM is also 0.5 g kg$^{-1}$ too humid, but because $L_vE$ is overestimated (see FB in Table 2). ETA and BT are too humid because $L_vE$ (similar as in MRF and BLA) is mixed in a shallower ABL. Since $L_vE$ is small, and thus convection is relatively strong, the CBL is forced by nonlocal mixing and thus the resulting $q$ profiles strongly rely on CBL top entrainment (Beljaars
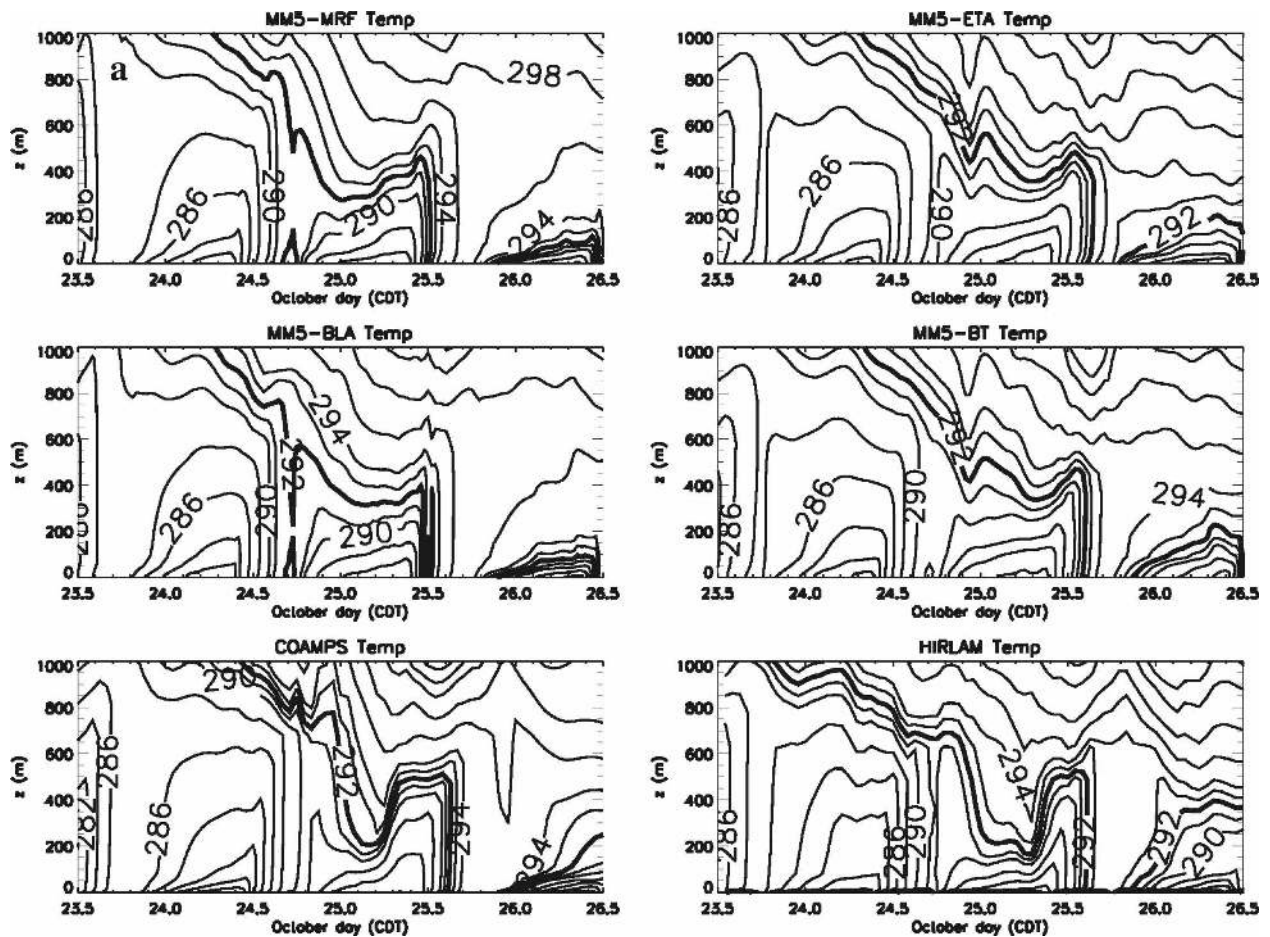
FIG. 5. Contour plots of (a) modeled potential temperature contour interval 1 K for $\theta < 288$ K and 2 K for $\theta > 288$ K, and (b) wind speed modulus for 1800 UTC 23 Oct–1800 UTC 26 Oct.

and Viterbo 1998). The MM5 schemes underestimate the stratification in the capping inversion, as found in HY01, while COAMPS and HIRLAM provide a sharper inversion. The length scale formulation for stable stratification that strongly reduces mixing is likely responsible for this effect. This also explains why HIRLAM (although a TKE scheme) is not as moist as ETA and BT.

### c. Stable boundary layer

Recalling that our current understanding of the SBL is limited, we may expect more spread between model results at night than during the day. Observations in the intermittent night (23–24 October) show a temperature inversion of 8 K near the surface, which is only clearly represented by COAMPS and BT near sunrise (not shown). The effect of the warmer CBL remains at night in MM5-BLA and MM5-MRF with higher temperatures.

In general the wind speed profiles are well represented, but a sharp 12 m s$^{-1}$ LLJ at 0700 UTC 24 October is predicted too late by all schemes, although COAMPS and BT, and (at 1100 UTC) also HIRLAM show slightly better performance than the other schemes.

The characteristic LLJ in the turbulent night (24–25 October) is reasonably forecast in strength by COAMPS, although it overestimates the LLJ altitude and underestimates $U$ in the residual layer (Fig. 7a). The BT and ETA forecast a LLJ over a deep layer, although weaker than observed. BLA extensively mixes the LLJ over an even deeper layer. HIRLAM underestimates the LLJ speed. The wind direction is forecast well, although BLA and MRF provide 10°–20° less backing near the surface than observed (Fig. 7b). The $\theta$ profiles are in reasonable agreement with the observations (not shown). Note that during the 0700 UTC 25 October sounding, the spread of the modeled wind speed profiles was less than in the 1100 UTC sounding.
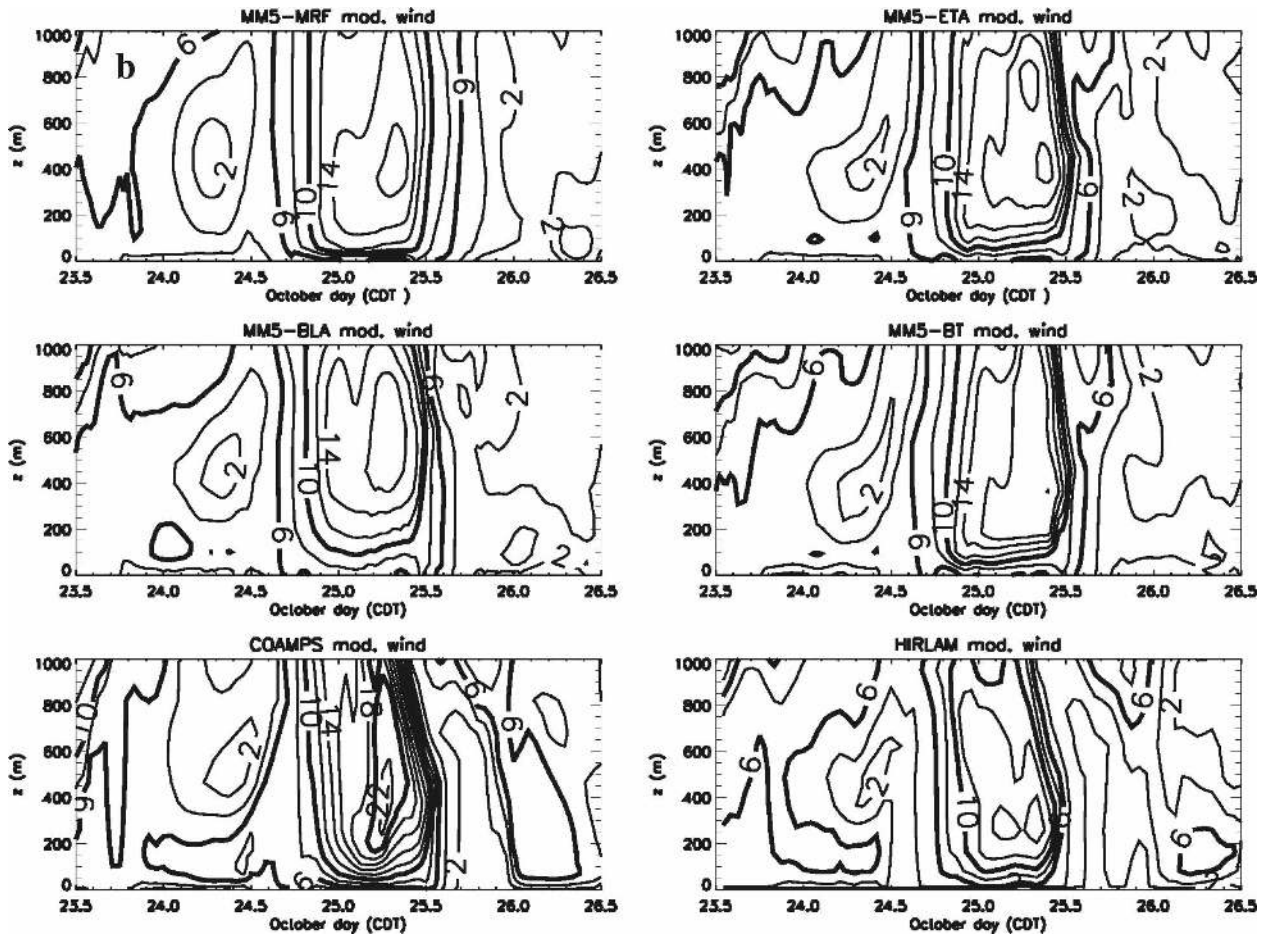
FIG. 5. (*Continued*)

To examine the impact of resolution on the ability to resolve LLJ, we performed a sensitivity study with MM5-BT in which we added 10 layers in the lowest 500 m. Unfortunately, this gave no improvement. The literature suggests several possible physical mechanisms for LLJ formation (Zhong et al. 1996). The explanation by Blackadar of an inertial oscillation after collapse of the turbulent friction at sunset is less probable here because $u_*$ is large at night. Fast and McCorcle (1990) show that differences of evaporation rates along a slope can be an important LLJ forcing. However, in that case we would expect a stronger jet during the other nights as well. Last, differential cooling between the slope and the adjacent air at constant height can generate a thermal wind $V_T$ (Stull 1988), in this case to the north. During the two first nights the horizontal temperature gradients are similar. However, during the first night the background wind speed is from the northeast, and thus opposes $V_T$. On the contrary, on the second night $V_T$ adds to the southern background wind. Since this

phenomenon is driven by the terrain slope, it should be well represented in the model topography.

In the radiative driven night (25–26 October), the underestimated surface cooling in MM5 is even more pronounced than during the intermittent night (24–25 October), with an observed inversion strength of 16 K over 100 m (Fig. 7c). ETA, BT, and HIRLAM are too cold above 50 m AGL, the remnants of the cool CBL. COAMPS performs well in this night, with a curvature of the $\theta$ profile similar to the observed, although somewhat weaker and more realistic. The $\theta$ jump between the surface and the first model level seems exaggerated.

### d. Impact of domain size

Next we focus on the impact of the selected domain size on the LLJ representation. The Great Plains are slightly sloping toward the northwest direction. Rapid surface cooling on the slope causes a strong temperature gradient in the air at the same altitude. Accordingly, a LLJ develops according to the thermal wind
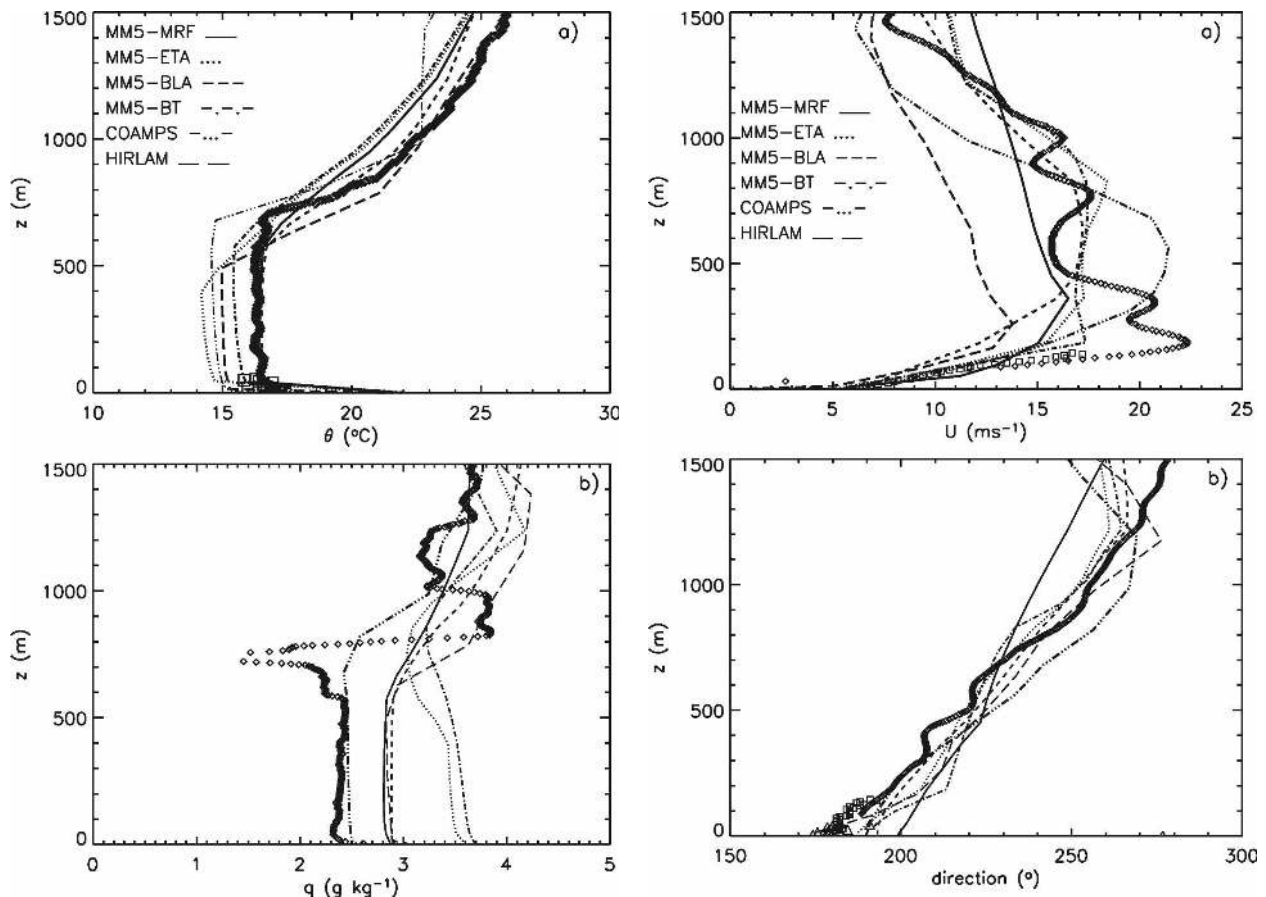
FIG. 6. Profiles of observed (diamonds are radiosonde observations; squares are tower observations) and simulated (a) potential temperature and (b) specific humidity for 1900 UTC 24 Oct.

relation. A sufficiently large area of this sloping terrain should be present in the model. Running the case with COAMPS and MM5 with finer resolution (27, 9, 3, and 1 km), but a smaller domain (810 km × 810 km) revealed a LLJ with at maximum 12 m s$^{-1}$ instead of 17 m s$^{-1}$ for all schemes. This is probably caused by the ECMWF boundary conditions, which showed a LLJ speed of only 11 m s$^{-1}$. With a small domain the LAMs are too much constrained to the boundaries. Note that normally the Great Plains jet is a band of high wind speed, and thus a single radiosonde profile gives limited insight. It is therefore worthwhile to note that a stronger LLJ was found elsewhere in the MM5 domain.

## 6. Sensitivity to radiation schemes

The previous section showed that model prediction of the near-surface temperature at night is erroneous. Examining the sensitivity of the results to the choice of the radiation scheme is useful since radiation plays an
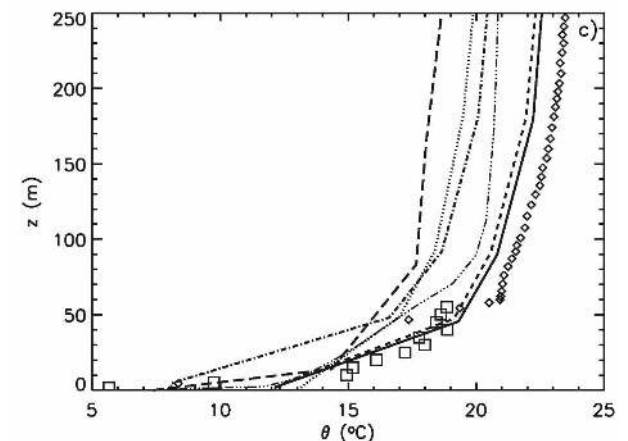


FIG. 7. Modeled and observed (diamond is sounding, square is minisodar, and triangle is 60-m tower) (a) modulus wind speed and (b) wind direction (1100 UTC 25 Oct) and (c) modeled and observed (diamonds are radiosonde observations; squares are tower observations) potential temperature for 0700 UTC 26 Oct.

important role in the surface cooling at night. To explore this sensitivity, the simulations with MM5-MRF and MM5-ETA have been repeated using the RRTM and CCM3 radiation transfer schemes in addition to the reference CLOUD scheme. The CLOUD scheme only
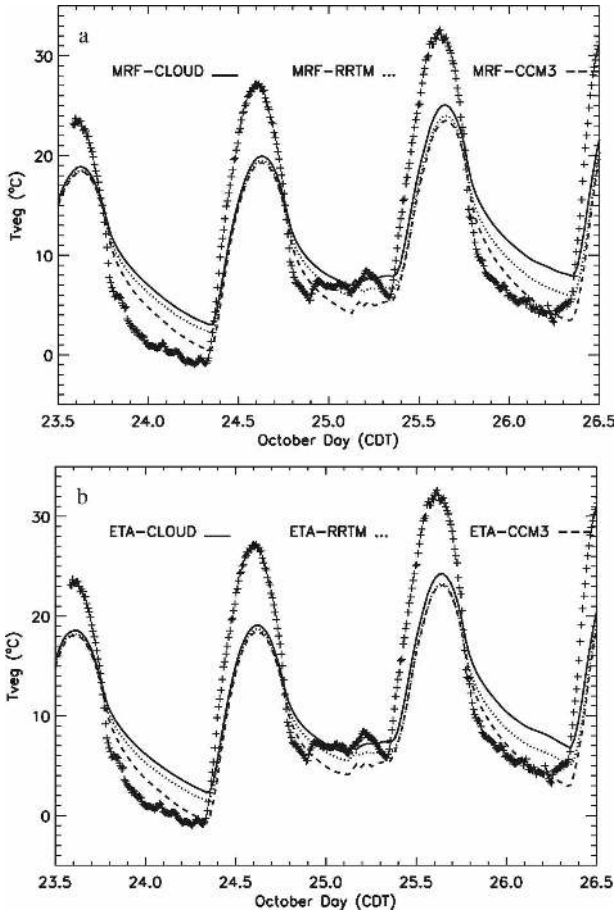
FIG. 8. Modeled (MM5) and observed surface vegetation temperature, as modeled with the CLOUD, RRTM, and CCM3 radiation scheme in combination with the (a) MRF and (b) ETA boundary layer scheme.

TABLE 3. Statistical model evaluation for the sensitivity to the radiation scheme.

| | | Bias | MAE | RMSE | FB | Corr | IoA |
|---|---|---|---|---|---|---|---|
| $T_{veg}$ | MRF-cloud | 0.35 | 4.65 | 5.34 | 0.03 | 0.88 | 0.92 |
| $u_*$ | MRF-cloud | 0.06 | 0.09 | 0.11 | 0.32 | 0.68 | 0.80 |
| $H$ | MRF-cloud | −4.74 | 24.81 | 36.73 | −0.18 | 0.87 | 0.94 |
| $L_v E$ | MRF-cloud | 2.47 | 8.07 | 10.90 | 0.19 | 0.77 | 0.88 |
| $L^\downarrow$ | MRF-cloud | 5.49 | 12.40 | 16.71 | 0.02 | 0.73 | 0.82 |
| $L^\uparrow$ | MRF-cloud | −0.67 | 20.34 | 24.28 | 0.00 | 0.89 | 0.93 |
| $T_{veg}$ | MRF-RRTM | −0.72 | 4.39 | 5.37 | −0.06 | 0.87 | 0.92 |
| $u_*$ | MRF-RRTM | 0.05 | 0.09 | 0.11 | 0.28 | 0.66 | 0.81 |
| $H$ | MRF-RRTM | −8.97 | 25.26 | 38.07 | −0.37 | 0.86 | 0.93 |
| $L_v E$ | MRF-RRTM | 0.94 | 7.55 | 10.53 | 0.08 | 0.77 | 0.89 |
| $L^\downarrow$ | MRF-RRTM | −9.44 | 14.72 | 17.97 | −0.03 | 0.70 | 0.79 |
| $L^\uparrow$ | MRF-RRTM | −6.15 | 19.52 | 25.21 | −0.02 | 0.88 | 0.93 |
| $T_{veg}$ | MRF-CCM3 | −1.86 | 4.17 | 5.36 | −0.18 | 0.88 | 0.92 |
| $u_*$ | MRF-CCM3 | 0.05 | 0.09 | 0.11 | 0.27 | 0.64 | 0.80 |
| $H$ | MRF-CCM3 | −11.00 | 26.47 | 38.77 | −0.47 | 0.86 | 0.93 |
| $L_v E$ | MRF-CCM3 | 0.21 | 7.29 | 10.61 | 0.02 | 0.76 | 0.88 |
| $L^\downarrow$ | MRF-CCM3 | −35.38 | 37.48 | 39.80 | −0.13 | 0.62 | −0.01 |
| $L^\uparrow$ | MRF-CCM3 | −11.71 | 19.16 | 26.06 | −0.03 | 0.89 | 0.92 |
| $V$ | ETA-cloud | −0.49 | 4.46 | 5.32 | −0.04 | 0.88 | 0.92 |
| $u_*$ | ETA-cloud | 0.05 | 0.08 | 0.10 | 0.30 | 0.78 | 0.86 |
| $H$ | ETA-cloud | −5.57 | 23.94 | 36.02 | −0.21 | 0.87 | 0.94 |
| $L_v E$ | ETA-cloud | 7.46 | 11.49 | 16.60 | 0.48 | 0.77 | 0.72 |
| $L^\downarrow$ | ETA-cloud | 1.93 | 11.13 | 16.19 | 0.01 | 0.70 | 0.83 |
| $L^\uparrow$ | ETA-cloud | −4.99 | 19.70 | 24.71 | −0.01 | 0.89 | 0.93 |
| $T_{veg}$ | ETA-RRTM | −1.50 | 4.29 | 5.49 | −0.14 | 0.88 | 0.92 |
| $u_*$ | ETA-RRTM | 0.05 | 0.07 | 0.09 | 0.27 | 0.78 | 0.86 |
| $H$ | ETA-RRTM | −9.10 | 24.25 | 37.27 | −0.37 | 0.87 | 0.94 |
| $L_v E$ | ETA-RRTM | 5.63 | 10.43 | 15.26 | 0.39 | 0.76 | 0.76 |
| $L^\downarrow$ | ETA-RRTM | −11.97 | 16.94 | 19.65 | −0.04 | 0.68 | 0.75 |
| $L^\uparrow$ | ETA-RRTM | −10.14 | 19.42 | 26.37 | −0.03 | 0.89 | 0.92 |
| $T_{veg}$ | ETA-CCM3 | −2.55 | 4.09 | 5.53 | −0.25 | 0.89 | 0.92 |
| $u_*$ | ETA-CCM3 | 0.04 | 0.07 | 0.09 | 0.25 | 0.77 | 0.87 |
| $H$ | ETA-CCM3 | −11.04 | 24.35 | 37.58 | −0.47 | 0.87 | 0.93 |
| $L_v E$ | ETA-CCM3 | 4.81 | 9.86 | 15.11 | 0.34 | 0.76 | 0.77 |
| $L^\downarrow$ | ETA-CCM3 | −36.94 | 38.91 | 41.29 | −0.14 | 0.60 | −0.08 |
| $L^\uparrow$ | ETA-CCM3 | −15.18 | 19.28 | 27.35 | −0.04 | 0.90 | 0.91 |

considers the interaction of radiation with water vapor and $CO_2$, whereas RRTM represents a detailed absorption spectrum of $CO_2$, $CH_4$, $NO_x$, and $O_3$. In CCM3 the longwave radiative effects of the greenhouse gases $CO_2$, $O_3$, $H_2O$, $CH_4$, $N_2O$, CFC11, and CFC12 are treated using broadband approximations, and an 18-band δ-Eddington approximation is used for solar radiation. Details on the different radiation transfer schemes are beyond the scope of this paper but can be found in Dudhia (1989), Mlawer et al. (1997), and Kiehl et al. (1998) for the CLOUD, RRTM, and CCM3 schemes, respectively. As shown by Guichard et al. (2003), we expect the latter scheme to produce smaller $L^\downarrow$, permitting more nocturnal surface cooling under clear-sky conditions.

Figure 8 shows that the forecast $T_{veg}$ at night, using either MRF or ETA, depends strongly on the chosen radiation scheme. The CLOUD radiation scheme always predicts higher nighttime $T_{veg}$, while the CCM3

radiation scheme gives lower, and more realistic $T_{veg}$. The difference between the two schemes is 2.5, 2.5, and 5 K at maximum for the three nights, respectively. The prediction of $T_{veg}$ with ETA-CCM3 is rather good during the radiative night (25–26 October) and may be considered as an optimal parameterization for strong SBLs. However, Table 3 reveals that the RRTM scheme and CCM3 scheme predict a cooler surface due to underestimation of $L^\downarrow$ and an overestimation of the magnitude of $Q^*$. This is a typical case of "getting the right answer for the wrong reason." Note that the forecast $T_{veg}$ is insensitive to the choice of the radiation scheme during daytime for both turbulence schemes.

Thus, SBL modeling is not only very sensitive to the degree of turbulent mixing (e.g., Viterbo et al. 1999), the coupling between the atmosphere and the land surface (S06), but certainly it also depends on the radiation parameterization (Ha and Mahrt 2003).

## 7. Alternative land surface scheme and turbulent mixing

Above we found that models with a vegetation layer and with limited turbulent mixing favor surface cooling in comparison with observations. Since the MM5-MRF model is computationally fast and has a good performance during daytime, we try to improve this model at night, and thus the model's representation of the full diurnal cycle. Two modifications are proposed:

1) Several studies showed the importance of a correct representation of the atmosphere–land–interaction (Holtslag and de Bruin 1988; van de Wiel 2002; S06). The latter study was able to predict $T_{veg}$ and energy balance components satisfactorily for the same days as examined here. This was achieved by using a vegetation surface layer with small heat capacity, and to ensure that the soil was able to deliver heat to the surface sufficiently fast. This is especially important for quiet periods where turbulence vanishes and net radiation $Q*$ must equal $G$. To improve the representation of the feedback with the soil in MM5-MRF, the original description of $G$ in MM5-MRF:

$$G = 1.18\Omega C_g(T_g - T_M), \qquad (8)$$

has been replaced by

$$G = \Lambda(T_{veg} - T_g), \qquad (9)$$

where $T_g$ is the surface soil surface temperature, $T_M$ is the 24-h mean 2-m air temperature used as the deep soil temperature, and $\Omega$ is the earth's angular velocity. This modification coincides with the implementation of a vegetation layer with a small heat capacity $C_{veg}$. We choose $C_{veg} = 2 \times 10^3$ J m$^{-2}$ K$^{-1}$ and surface resistance $\Lambda = 5.9$ W m$^{-2}$ K$^{-1}$ as observed by S06 for CASES-99. Originally $C_g = 2 \times 10^6$ J m$^{-2}$ K$^{-1}$, so this modification enables the modeled $T_{veg}$ to react more quickly on a change of the net radiation. Figure 9 summarizes the modified scheme conceptually.

2) The original MM5-MRF scheme uses a prescribed $K$ profile function form, where $K$ depends on $u_*$ and $h$. However, Nieuwstadt (1984) showed that turbulent mixing in the SBL is local and therefore $K$ based on the surface friction seems to be less realistic (Mahrt and Vickers 2003), especially when we realize that the model keeps surface $u_*$ artificially large for quiet conditions. Additionally, S06 found a very good performance for CASES-99 using a local turbulence scheme. Therefore, we replace the original scheme with a local ABL scheme. Herein $l = kz$, and flux-profile relation $\varphi$ based on the local scaling
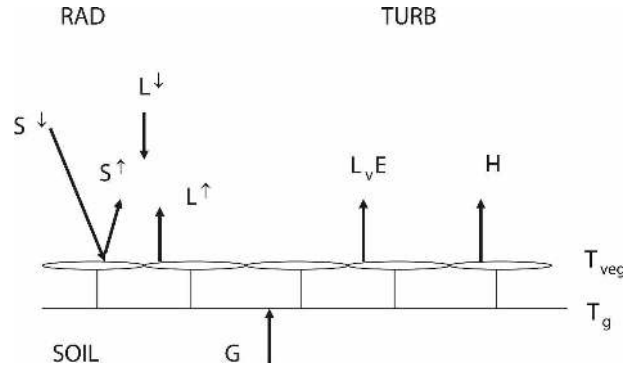


FIG. 9. Illustration of the interaction between the energy fluxes by different physical processes in the SBL for the revised scheme in MM5-MRF, as extended with the surface *vegetation* temperature.

hypothesis (Holtslag and Nieuwstadt 1986; $\beta = 5$, $\alpha = 0.8$, $\zeta = z/\Lambda$, with $\Lambda$ the local Obukhov length (Duynkerke 1991):

$$\varphi(\zeta) = 1 + \beta\zeta(1 + \beta\zeta/\alpha)^{\alpha-1} \qquad (10)$$

for $\theta$, $U$, and $q$. This $\varphi$ allows for some turbulent transport for $\zeta > 1$, but less than in large-scale models (Viterbo et al. 1999). Moreover, in both simulations updates of the surface fluxes due to updated surface temperature were skipped since they were originally done with the $T_g$ rather than with $T_{veg}$.

Figure 10a shows the model results for $T_{veg}$ for the modified scheme. At first, during all nights the modifications give a $T_{veg}$ less than the reference scheme, and always better in agreement with the observations. Especially for quiet nights the cooling is 6 K stronger than for the reference run. The $T_{veg}$ also improves during the daytime ($\sim$3 K), although the model is still too cold.

The friction velocity (Fig. 10b) with the modified schemes improves, especially after the day–night transition. During this stage of the diurnal cycle, the rapid surface cooling in the model enhances the stratification also rapidly, and consequently limits turbulent mixing. For the radiative night (25–26 October), $u_*$ improves strongly in the first half of the night relative to the reference run. Interestingly, the scheme for which only the vegetation layer has been altered shows a $u_*$ increase at around 0100 central daylight time (CDT). The low $u_*$ ensures a decoupling of the atmosphere from the surface. As such, the flow aloft accelerates, increasing the wind shear, and finally the flow recouples to the surface, and increases $u_*$. This effect is smaller when the local mixing scheme is also used.

The strong and unrealistic revival of $u_*$ might occur because the flow acceleration aloft starts at a different
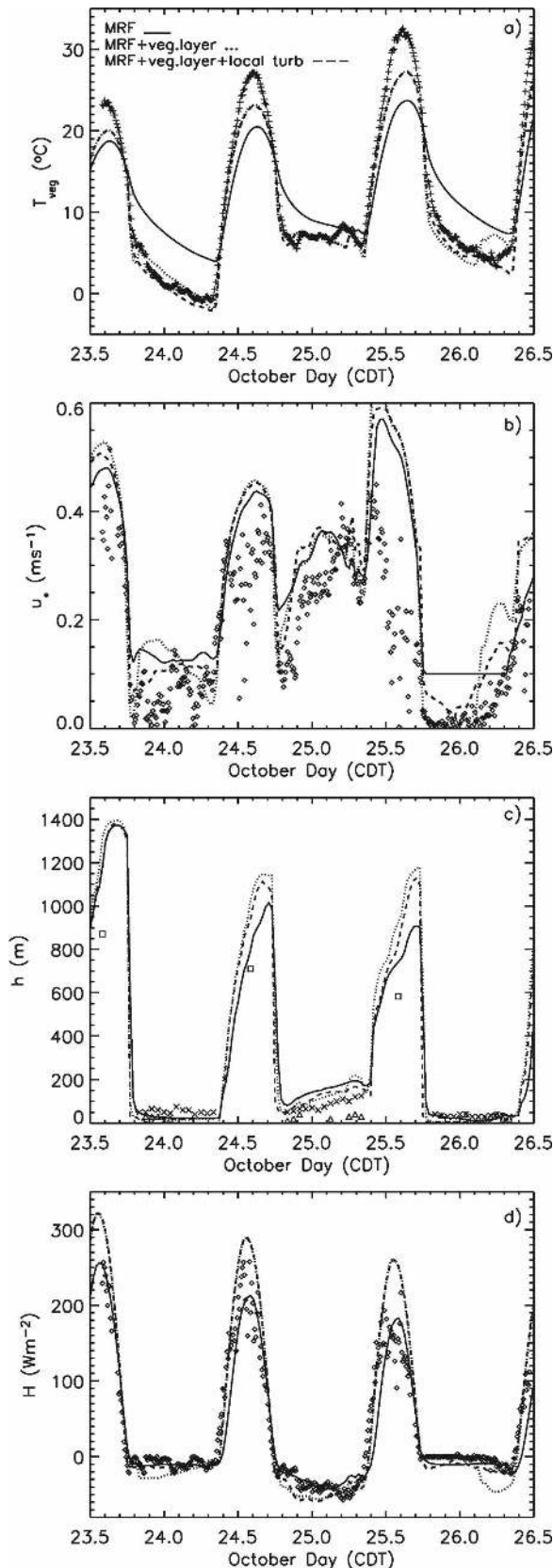
level than in reality, which might be due to limited resolution close to the surface. In general the addition of the local mixing scheme reduces the turbulence intensity relative to the simulation that only introduced the vegetation layer.

Figure 10c shows that for the windy night (24–25 October) the dynamical development of the SBL height agrees with the observations and increases with time. However, $h$ is still overestimated, but less than for the reference runs. Unfortunately, the CBL deepens compared with the reference runs. This is because of an increased $H$ during the day. The calculation of the CBL height in MM5-MRF might be reconsidered to circumvent CBLs that are too deep.

Considering the $\theta$ and $U$ profiles (Fig. 11), we find that improvements 1) and 2) provide realistic cooling during weak wind conditions (23–24 and 25–26 October) and the LLJ is better represented. Unfortunately, the overestimated daytime heating provides warmer and deeper CBLs, and therefore the temperature profile is biased. However, the modeled and observed SBL *structure* corresponds rather well, especially when local mixing is utilized. The simulations with the Duynkerke (1991) turbulence scheme provide typically a shallower and more realistic SBL than with the $K$ profile method. Additionally, the surface inversion is several degrees stronger than for the reference scheme (Fig. 11c). With the new schemes, also $U$ is larger (Fig. 11b) in the residual layer because of enhanced daytime momentum mixing. The wind speed maximum is sharper, with a stronger wind speed, and at a lower altitude.

Although the model results do not perfectly match the observations, the updated schemes show some clear and characteristic improvements for the modeled SBL profiles, and surface fluxes.

## 8. Conclusions and recommendations

This study examines the performance of three limited-area models (MM5, COAMPS, and HIRLAM) for three diurnal cycles with contrasting stable boundary layers during the CASES-99 experimental campaign. The first night is classified as intermittently turbulent, the second is continuously turbulent, and the last night

←

FIG. 10. (a) Modeled surface temperature, (b) friction velocity, and (c) boundary layer height and (d) surface sensible heat flux with the MM5-MRF scheme (full line), MM5-MRF updated with a vegetation layer (dotted line), and MM5-MRF updated with a vegetation layer + local mixing scheme (dashed line). Observations labels are as in Fig. 4.
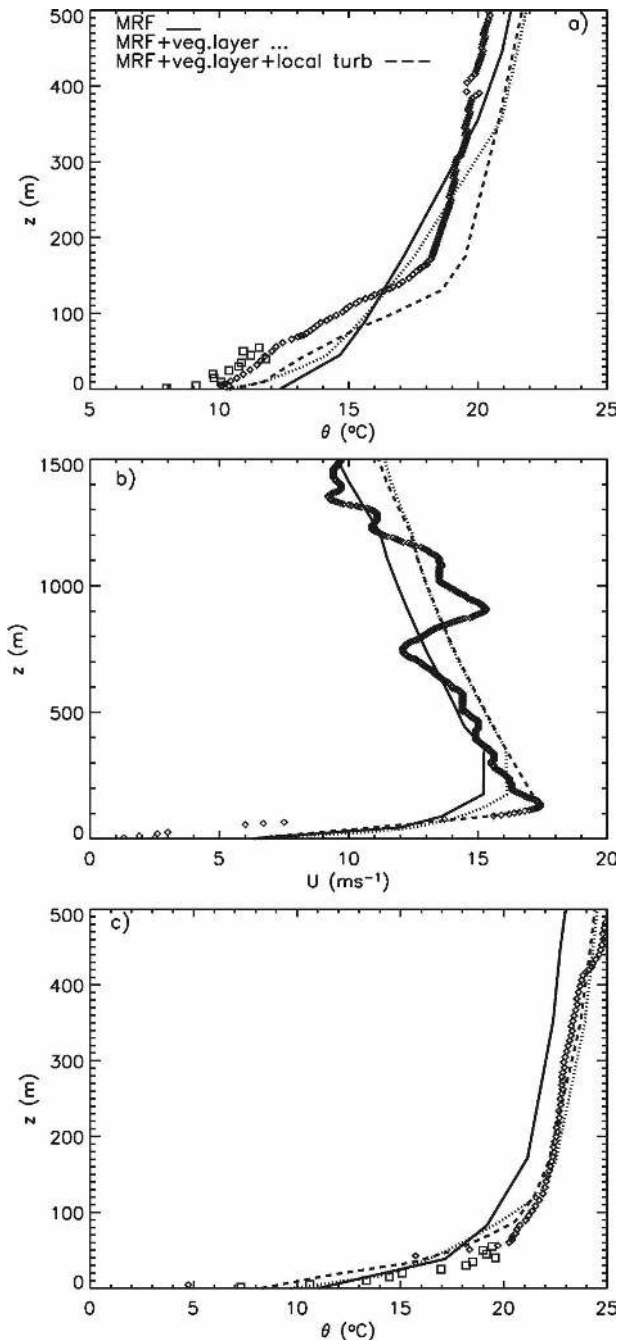
FIG. 11. Modeled and observed (a) potential temperature and (b) wind speed for 0700 UTC 25 Oct, and modeled and observed (c) potential temperature for 0700 UTC 26 Oct for the reference MRF scheme (full line), MRF with a vegetation layer (dotted line), and MRF with vegetation layer + local mixing scheme by Duynkerke (1991) (dashed line).

is weakly turbulent. The strategy was to identify common deficiencies of these schemes and to identify conditions when certain schemes are beneficial.

All schemes underestimate the diurnal temperature

cycle amplitude and the near-surface stability at night. None of the parameterizations was able to represent the surface radiation and turbulent fluxes, the wind speed and temperature profiles, and the boundary layer height correctly during the full diurnal cycle. Schemes with local mixing provide a more realistic representation of the nighttime boundary layer, especially for weak winds, and when the asymptotic length scale is based on the flow properties. Moreover, the nighttime low-level jet is hard to reproduce, and we find a clear dependence on the chosen model domain size. Too-small horizontal model domains provide an LLJ speed underestimation, because its generating mechanism (according to the thermal wind relation) is underestimated in that case. With a small domain, the modeled profiles depend too much on the boundary conditions by ECMWF, which underestimates the LLJ speed.

Additional sensitivity tests with different radiation schemes revealed large differences of the net cooling rate between these schemes and consequently to the forecast surface temperature, especially for calm nights. This was mainly due to underestimated incoming long-wave radiation.

Encouraged by earlier 1D results (e.g., S06) and to improve these results we implemented a new scheme for the stable boundary layer in MM5-MRF. The scheme introduces a vegetation layer with a small heat capacity, a realistic formulation for the soil heat flux, and a mixing scheme based on the local similarity hypothesis for stable conditions. The updated scheme improves the representation of the diurnal temperature range and the vertical structure of the forecast profiles, especially for calm nights. This also gives more realistic shallow boundary layers with stronger inversions.

## APPENDIX

## Model Description

### a. Surface layer

Surface fluxes of heat momentum are calculated with Eq. (1) with the transfer coefficients specified below (here $z_a$ is the first atmospheric model level and $\psi_m$ and $\psi_n$ are the stability corrections for momentum and heat, respectively):

1) MM5-MRF, MM5-ETA, MM5-BLA (Braun and Tao 2000):

$$C_\theta = k^2[\ln(z/z_0) - \psi_m]^{-1}[\ln(z/z_0) - \psi_h]^{-1} \quad \text{and}$$

$$C_D = k^2(\ln(z/z_0) - \psi_m)^{-2}, \quad \text{(A1)}$$

2) MM5-BT (with $b = c = 5$):

$$C_\theta = \frac{k^2}{\ln^2(z/z_0)}\left[1 - \frac{3b\text{Ri}_b}{1 + \frac{3bck^2}{\ln^2(z_a/z_0)}\sqrt{-\frac{z_a\text{Ri}_b}{z_0}}}\right]$$

and

$$C_D = \frac{k^2}{\ln^2(z/z_0)}\left[1 - \frac{2b\text{Ri}_b}{1 + \frac{3bck^2}{\ln^2(z_a/z_0)}\sqrt{-\frac{z_a\text{Ri}_b}{z_0}}}\right],$$

$$\text{(A2)}$$

3) COAMPS (Hodur 1997):

$$C_D = \frac{k^2 f_m(z_a/z_0, \text{Ri})}{\ln^2(z_a/z_0)} \quad \text{and} \quad C_\theta = \frac{k^2 f_h(z_a/z_0, \text{Ri})}{R\ln^2(z/z_0)} \quad \text{with}$$

$$R = 0.74, \quad \text{and} \quad \text{(A3)}$$

4) HIRLAM (Undén et al. 2002):

$$C_{m,h} = \frac{k^2}{\ln^2(z/z_0)}\left[1 + \frac{\ln(z_{0m}/z_{0h})}{\ln(z/z_{0m})}\right]^{-1}$$

$$\times f_{m,h}\left(\frac{z}{z_0}, \frac{z}{z_{0h}}, \text{Ri}_b\right), \quad \text{with} \quad \text{(A4)}$$

$$f_m = 1 + \left(1 + \frac{10\text{Ri}}{\sqrt{1 + \text{Ri}}}\right)^{-1} \quad \text{and}$$

$$f_h = 1 + \frac{1}{1 + 10\text{Ri}\sqrt{1 + \text{Ri}}}\left[\frac{\ln(z/z_0)}{\ln(z/z_{0h})}\right]. \quad \text{(A5)}$$

### b. Boundary layer

The ABL scheme is characterized by the specification of the eddy diffusion coefficient for momentum ($K_m$) and heat ($K_h$) as follows:

1) MM5-MRF:

$\overline{w\theta} = -K_h[(\partial\theta/\partial z) - \gamma_c]$, where $\gamma_c = 7.8\overline{w\theta_s}/(w_s h)$, with $w_s$ as an appropriate velocity scale, with $\gamma_c = 0$ at night [herein $K_h = kw_s z(1 - z/h)^2$ and $K_m = K_h\text{Pr} = K_h(\varphi_h/\varphi_m + 0.78k)$ with Prandtl number Pr],

2) MM5-ETA:

$$K_{m,h} = S_{M,H}(\text{Ri}_{\text{flux}})L_{MY}\sqrt{E} \quad \text{and}$$

$$L_{MY} = kz/(1 + kz/l_\infty), \quad \text{(A6)}$$

3) MM5-BT:

$$K_{m,h} = L_{MY}\sqrt{E}f_{m,h}, \quad \text{where}$$

$$L_{MY} = kz/(1 + kz/l_\infty), \quad \text{(A7)}$$

$$f_m = \frac{1}{1 + 2b\text{Ri}(1 + d\text{Ri})^{-(1/2)}}, \quad \text{and}$$

$$f_h = \frac{1}{1 + 3b\text{Ri}(1 + d\text{Ri})^{-(1/2)}}, \quad \text{with}$$

$$b = 5 \text{ and } d = 5, \quad \text{(A8)}$$

4) MM5-BLA:

for CBL model layer $j$,

$$\overline{w\theta}_j = \overline{w\theta}_1 - \overline{m}\int_{z_1}^{z_j}[\theta_1 - \theta(z)]\,dz \quad \text{(A9)}$$

with

$$\overline{m} = \overline{w\theta_v}/0.8\int_{z_1}^{z_m}\theta_1 - \theta(z)\,dz, \quad \text{and}$$

for nocturnal conditions,

$$K_h = K_0 + |\partial U/\partial z|l^2 f(\text{Ri}), \quad \text{(A10)}$$

where $f(\text{Ri}) = [1 + 10\text{Ri}(1 + 8\text{Ri})]^{-1}$ for $\text{Ri} > 0$, and $K_0$ is background diffusion,

5) COAMPS:

as for MM5-ETA, but

$$l_\infty = 0.1\int_0^h z\sqrt{E}\,dz/\int_0^h \sqrt{E}\,dz, \quad \text{and} \quad \text{(A11)}$$

6) HIRLAM:

$$K_{m,h} = l\sqrt{E}, \quad \text{(A12)}$$

with $l$ as in Eqs. (5)–(9).

### c. Surface scheme

All models solve the heat budget at the surface, but employ different $C_{\text{surf}}$ values

$$C_{\text{surf}}\partial T_{\text{veg}}/\partial t = Q^* - G - H - L_v E \quad \text{(A13)}$$

as follows:

1) MM5-MRF, MM5-ETA, MM5-BLA:

$$G = 1.18\Omega C_g(T_g - T_M), \quad \text{(A14)}$$

2) MM5-BT: Deardorff (1978),

3) COAMPS:

$$G = 1.8.10^{-4}(T_g - T_M), \quad \text{and} \quad \text{(A15)}$$

4) HIRLAM: ISBA scheme (Noilhan and Planton 1989; Noilhan and Mahfouf 1996),

$$C_{surf} = \left( \frac{1 - f_{veg}}{C_g} + \frac{f_{veg}}{C_{veg}} \right)^{-1}, \qquad (A16)$$

with $C_{veg} = 2 \times 10^5$ J m$^{-1}$ K$^{-1}$ (the scheme uses a force–restore method in the deep soil, for which the coefficients are calibrated against a high-resolution soil model).

## REFERENCES

Aalto, T., J. Hatakkal, U. Karstens, M. Aurela, T. Thum, and A. Lohila, 2006: Modeling atmospheric CO$_2$ concentration profiles and fluxes above sloping terrain at a boreal site. *Atmos. Chem. Phys.,* **6,** 303–314.

Banta, R. M., R. K. Newsom, J. K. Lundquist, Y. L. Pichugina, R. L. Coulter, and L. Mahrt, 2002: Nocturnal low-level jet characteristics over Kansas during CASES-99. *Bound.-Layer Meteor.,* **105,** 221–252.

Beljaars, A. C. M., 1995: The impact of some aspects of the boundary layer scheme in the ECMWF model. *Proc. Seminar on Parametrization of Subgrid Scale Physical Processes,* Reading, United Kingdom, ECMWF, 125–161.

——, 2001: Issues in boundary layer parameterization for large scale models. *Proc. Seminar on Key Issues in the Parametrization of Subgrid Physical Processes,* Reading, United Kingdom, ECMWF, 71–87.

——, and P. Viterbo, 1998: Role of the boundary layer in a numerical weather prediction model. *Clear and Cloudy Boundary Layers,* A. A. M. Holtslag and P. G. Duynkerke, Eds., Royal Netherlands Academy of Arts and Sciences, 372 pp.

Berg, L. K., and S. Zhong, 2005: Sensitivity of MM5 simulated boundary layer characteristics to turbulence parameterization. *J. Appl. Meteor.,* **44,** 1467–1483.

Betts, A. K., 2001: The diurnal cycle over land. *Proc. Seminar on Key Issues in the Parametrization of Subgrid Physical Processes,* Reading, United Kingdom, ECMWF, 289–304.

Braun, S. A., and W. K. Tao, 2000: Sensitivity of high-resolution simulations of Hurricane Bob (1991) to planetary boundary layer parameterizations. *Mon. Wea. Rev.,* **128,** 3941–3961.

Bright, D. R., and S. L. Mullen, 2002: The sensitivity of the numerical of the Southwest Monsoon boundary layer to the choice of PBL turbulence parameterization in MM5. *Wea. Forecasting,* **17,** 99–114.

Burk, S. D., and W. T. Thompson, 1989: Vertically nested regional numerical weather prediction model with second-order closure physics. *Mon. Wea. Rev.,* **117,** 2305–2324.

Cassano, J. J., T. R. Parish, and J. C. King, 2001: Evaluation of turbulent surface flux parameterizations for the stable surface layer over Halley, Antarctica. *Mon. Wea. Rev.,* **129,** 26–46.

Couvreux, F., F. Guichard, J.-L. Redelsperger, C. Kiemle, V. Masson, J.-P. Lafore, and C. Flamant, 2005: Water vapour variability within a convective boundary-layer assessed by large-eddy simulations and IHOP-2002 observations. *Quart. J. Roy. Meteor. Soc.,* **131,** 2665–2693.

Cuxart, J., and Coauthors, 2006: Single-column model intercomparison for a stably stratified atmospheric boundary layer. *Bound.-Layer Meteor.,* **118,** 273–303.

Deardorff, J. W., 1978: Efficient prediction of ground surface tem-

perature and moisture with inclusion of a layer of vegetation. *J. Geophys. Res.,* **83,** 1889–1903.

Dudhia, J., 1989: Numerical study of convection observed during the winter monsoon experiment using a mesoscale two-dimensional model. *J. Atmos. Sci.,* **46,** 3077–3107.

——, and J. F. Bresch, 2002: A global version of the PSU–NCAR mesoscale model. *Mon. Wea. Rev.,* **130,** 2989–3007.

——, D. Gill, K. Manning, W. Wang, and C. Bruyere, 2000: PSU/NCAR mesoscale modeling system tutorial class notes and user's guide: MM5 modeling system version 3. Tech. Rep., National Center for Atmospheric Research, Boulder, CO, 138 pp. [Available online at http://www.mmm.ucar.edu/mm5/documents/.]

Duynkerke, P. G., 1991: Radiation fog: A comparison of model simulation with detailed observations. *Mon. Wea. Rev.,* **119,** 324–341.

Fast, J. D., and M. D. McCorcle, 1990: A two-dimensional numerical sensitivity study of the Great Plains low-level jet. *Mon. Wea. Rev.,* **118,** 151–163.

Guichard, F., D. B. Parsons, J. Dudhia, and J. Bresh, 2003: Evaluating mesoscale model predictions of clouds and radiation with SGP ARM data over a seasonal timescale. *Mon. Wea. Rev.,* **131,** 926–944.

Ha, K. J., and L. Mahrt, 2003: Radiative and turbulent fluxes in the nocturnal boundary layer. *Tellus,* **55A,** 317–327.

Hanna, S. R., and R. Yang, 2001: Evaluation of mesoscale models' simulations of near-surface winds, temperature gradients, and mixing depths. *J. Appl. Meteor.,* **40,** 1095–1104.

Harshvardhan, R. Davies, D. Randall, and T. Corsetti, 1987: A fast radiation parameterization for atmospheric circulation models. *J. Geophys. Res.,* **92,** 1009–1016.

Hodur, R. M., 1997: The Naval Research Laboratory coupled ocean/atmosphere mesoscale prediction system. *Mon. Wea. Rev.,* **125,** 1414–1430.

Holtslag, A. A. M., 2006: Preface: GEWEX Atmospheric Boundary-layer Study (GABLS) on stable boundary layers. *Bound.-Layer Meteor.,* **118,** 243–246.

——, and F. T. M. Nieuwstadt, 1986: Scaling the atmospheric boundary layer. *Bound.-Layer Meteor.,* **36,** 201–209.

——, and H. A. R. de Bruin, 1988: Applied modeling of the nighttime surface energy balance over land. *J. Appl. Meteor.,* **27,** 689–704.

——, and B. A. Boville, 1993: Local versus nonlocal boundary-layer diffusion in a global climate model. *J. Climate,* **6,** 1825–1842.

——, E. van Meijgaard, and W. C. de Rooy, 1995: A comparison of boundary layer diffusion schemes in unstable conditions over land. *Bound.-Layer Meteor.,* **76,** 69–95.

Hong, S. Y., and H. L. Pan, 1996: Nonlocal boundary layer vertical diffusion in a Medium-Range Forecast model. *Mon. Wea. Rev.,* **124,** 2322–2339.

Janjić, Z. I., 1990: The step-mountain coordinate: Physical package. *Mon. Wea. Rev.,* **118,** 1429–1443.

Kain, J. S., and J. M. Fritsch, 1993: Convective parameterization for mesoscale models: The Kain–Fritsch scheme. *The Representation of Cumulus Convection in Numerical Models, Meteor. Monogr.,* No. 24, Amer. Meteor. Soc., 165–170.

Kiehl, J. T., J. J. Hack, G. B. Bonan, B. A. Boville, D. L. Williamson, and P. J. Rasch, 1998: The National Center for Atmospheric Research Community Climate Model: CCM3. *J. Climate,* **11,** 1131–1149.

King, J. C., and W. M. Connolley, 1997: Validation of the surface energy balance over the Antarctic ice sheets in the U.K. Me-

teorological Office unified climate model. *J. Climate,* **10,** 1273–1287.

——, ——, and S. H. Derbyshire, 2001: Sensitivity of modelled Antarctic climate to surface flux and boundary-layer flux parameterizations. *Quart. J. Roy. Meteor. Soc.,* **127,** 779–794.

Kot, S. C., and Y. Song, 1998: An improvement of the Louis scheme for the surface layer in an atmospheric modeling system. *Bound.-Layer Meteor.,* **88,** 239–254.

Lenderink, G., and A. A. M. Holtslag, 2004: An updated length-scale formulation for turbulent mixing in clear and cloudy boundary layers. *Quart. J. Roy. Meteor. Soc.,* **130,** 3405–3428.

Louis, J. F., 1979: A parametric model of vertical eddy fluxes in the atmosphere. *Bound.-Layer Meteor.,* **17,** 187–202.

Mahrt, L., 1998: Stratified atmospheric boundary layers and breakdown of models. *Theor. Comput. Fluid Phys.,* **11,** 263–279.

——, 1999: Stratified atmospheric boundary layers. *Bound.-Layer Meteor.,* **90,** 375–396.

——, and D. Vickers, 2003: Formulation of fluxes in the stable boundary layer. *J. Atmos. Sci.,* **60,** 2538–2548.

——, J. Sun, W. Blumen, T. Delany, and S. Oncley, 1998: Nocturnal boundary-layer regimes. *Bound.-Layer Meteor.,* **88,** 255–278.

Mellor, G. L., and T. Yamada, 1974: A hierarchy of turbulence closure models for planetary boundary layers. *J. Atmos. Sci.,* **31,** 1791–1806.

Mlawer, E. J., S. J. Taubman, P. D. Brown, M. J. Iacono, and S. A. Clough, 1997: Radiative transfer for inhomogeneous atmospheres: RRTM, a validated correlated-k model for the longwave. *J. Geophys. Res.,* **102** (D14), 16 663–16 682.

Nieuwstadt, F. T. M., 1984: The turbulent structure of the stable, nocturnal boundary layer. *J. Atmos. Sci.,* **41,** 2202–2216.

Noilhan, J., and S. Planton, 1989: A simple parameterization of land surface processes for meteorological models. *Mon. Wea. Rev.,* **117,** 536–549.

——, and J. F. Mahfouf, 1996: The ISBA land surface parameterisation scheme. *Global Planet. Change,* **13,** 145–159.

Poulos, G. S., and Coauthors, 2002: CASES-99: A comprehensive investigation of the stable nocturnal boundary layer. *Bull. Amer. Meteor. Soc.,* **83,** 555–581.

Savijärvi, H., 1990: Fast radiation parameterization schemes for mesoscale and short-range forecast models. *J. Appl. Meteor.,* **29,** 437–447.

——, and J. Kauhanen, 2001: High resolution numerical simulations of temporal and vertical variability in the stable wintertime boreal boundary layer: A case study. *Theor. Appl. Climatol.,* **70,** 97–103.

Song, J., K. Liao, R. L. Coulter, and B. M. Lesht, 2005: Climatology of the low-level jet at the Southern Great Plains atmospheric boundary layer experiments site. *J. Appl. Meteor.,* **44,** 1593–1606.

Steeneveld, G. J., A. A. M. Holtslag, and H. A. R. de Bruin, 2005: Fluxes and gradients in the convective surface layer and the possible role of boundary-layer depth and entrainment flux. *Bound.-Layer Meteor.,* **116,** 237–252.

——, B. J. H. van de Wiel, and A. A. M. Holtslag, 2006: Modeling the evolution of the atmospheric boundary layer coupled to the land surface for three contrasting nights in CASES-99. *J. Atmos. Sci.,* **63,** 920–935.

Stull, R. B., 1988: *An Introduction to Boundary Layer Meteorology.* Kluwer Academic, 666 pp.

Tijm, A. B. C., 2004: Tuning CBR. *HIRLAM Newsl.,* **46,** 18–28.

Tjernström, M., M. Zagar, and G. Svensson, 2004: Model simulations of the arctic atmospheric boundary layer from the SHEBA year. *Ambio,* **33,** 221–227.

Troen, I. B., and L. Mahrt, 1986: A simple model of the atmospheric boundary layer; sensitivity to surface evaporation. *Bound.-Layer Meteor.,* **37,** 129–148.

Undén, P., and Coauthors, 2002: HIRLAM-5 scientific documentation. HIRLAM-5 Project, SMHI, Norrkoping, Sweden, 146 pp. [Available online at http://www.hirlam.org/open/publications/SciDoc_Dec2002.pdf.]

van den Hurk, B. J. J. M., and A. A. M. Holtslag, 1997: On the bulk parameterisation of surface fluxes for various conditions and parameter ranges. *Bound.-Layer Meteor.,* **82,** 119–134.

van de Wiel, B. J. H., 2002: Intermittent turbulence and oscillations in the stable boundary layer over land. Ph.D. thesis, Wageningen University, Wageningen, Netherlands, 129 pp.

Vickers, D., and L. Mahrt, 2004: Evaluating formulations of the stable boundary layer height. *J. Appl. Meteor.,* **43,** 1736–1749.

Vilà-Guerau de Arellano, J., O. S. Vellinga, A. A. M. Holtslag, F. C. Bosveld, and H. Klein Baltink, 2001: Observational evaluation of PBL parameterization modeled by MM5. *11th PSU/NCAR Mesoscale Model Users's Workshop,* Boulder, Colorado, NCAR, 102–104. [Available online at http://www.mmm.ucar.edu/mm5/workshop/ws01/vila.pdf.]

Viterbo, P., A. Beljaars, J. F. Mahfouf, and J. Teixeira, 1999: The representation of soil moisture freezing and its impact on the stable boundary layer. *Quart. J. Roy. Meteor. Soc.,* **125,** 2401–2426.

Vogelezang, D. H. P., and A. A. M. Holtslag, 1996: Evaluation and model impacts of alternative boundary-layer height formulations. *Bound.-Layer Meteor.,* **81,** 245–269.

Willmott, C. J., 1982: Some comments on the evaluation of model performance. *Bull. Amer. Meteor. Soc.,* **63,** 1309–1313.

Zehnder, J. A., 2002: Simple modifications to improve fifth-generation Pennsylvania State University-National Center for Atmospheric Research mesoscale model performance for the Phoenix, Arizona, metropolitan area. *J. Appl. Meteor.,* **41,** 971–979.

Zhang, D. L., and W. Z. Zheng, 2004: Diurnal cycles of surface winds and temperatures as simulated by five boundary layer parameterizations. *J. Appl. Meteor.,* **43,** 157–169.

Zhong, S., and J. D. Fast, 2003: An evaluation of MM5, RAMS, and Meso Eta at sub-kilometer resolution using the VTMX field campaign data in the Salt Lake Valley. *Mon. Wea. Rev.,* **131,** 1301–1322.

——, ——, and X. Bian, 1996: A case study of the Great Plains low-level jet using wind profiler network data and a high-resolution mesoscale model. *Mon. Wea. Rev.,* **124,** 785–806.